Drug Design, Development and Therapy

Dovepress

open access to scientific and medical research

Open Access Full Text Article

ORIGINAL RESEARCH

Sinomenine Alleviates Rheumatoid Arthritis by Suppressing the PI3K-Akt Signaling Pathway, as Demonstrated Through Network Pharmacology, Molecular Docking, and Experimental Validation

Qingyang Liu[1,*], Jian Wang[2,*], Chunhui Ding[3], Ying Chu[1], Fengying Jiang[1], Yunxia Hu[4], Haifeng Li[2], Qiubo Wang[1]

[1]Department of Clinical Laboratory, Wuxi Ninth People's Hospital Affiliated to Soochow University, Wuxi, Jiangsu, 214000, People's Republic of China; [2]Department of Orthopedics, Wuxi Ninth People's Hospital Affiliated to Soochow University, Wuxi, Jiangsu, 214000, People's Republic of China; [3]Department of Pharmacy, Wuxi Ninth People's Hospital Affiliated to Soochow University, Wuxi, Jiangsu, 214000, People's Republic of China; [4]Department of Rheumatology and Immunology, The Affiliated Wuxi People's Hospital of Nanjing Medical University, Wuxi, Jiangsu, 214000, People's Republic of China

*These authors contributed equally to this work

Correspondence: Qiubo Wang, Department of Clinical Laboratory, Wuxi Ninth People's Hospital Affiliated to Soochow University, No. 999 Liang Xi Road, Binhu District, Wuxi, Jiangsu, 214000, People's Republic of China, Email wangqiubo2020@suda.edu.cn; Haifeng Li, Department of orthopedics, Wuxi Ninth People's Hospital Affiliated to Soochow University, No. 999 Liang Xi Road, Binhu District, Wuxi, Jiangsu, 214000, People's Republic of China, Email lihaifeng2008@suda.edu.cn

Purpose: Sinomenine (SIN) is commonly used in Traditional Chinese Medicine (TCM) as a respected remedy for rheumatoid arthritis (RA). Nevertheless, the therapeutic mechanism of SIN in RA remains incompletely understood. This study aimed to delve into the molecular mechanism of SIN in the treatment of RA.

Methods: The potential targets of SIN were predicted using the TCMSP server, STITCH database, and SwissTarget Prediction. Differentially expressed genes (DEGs) in RA were obtained from the GEO database. Enrichment analyses and molecular docking were conducted to explore the potential mechanism of SIN in the treatment of RA. In vitro and in vivo studies were conducted to validate the intervention effects of SIN on rheumatoid arthritis, as determined through network pharmacology analyses.

Results: A total of 39 potential targets associated with the therapeutic effects of SIN in RA were identified. Enrichment analysis revealed that these potential targets are primarily enriched in PI3K-Akt signaling pathway, and the molecular docking suggests that SIN may act on specific proteins in the pathway. Experimental results have shown that exposure to SIN inhibits cytokine secretion, promotes apoptosis, reduces metastasis and invasion, and blocks the activation of the PI3K-Akt signaling pathway in RA fibroblast-like synoviocytes (RA-FLS). Moreover, SIN treatment alleviated arthritis-related symptoms and regulated the differentiation of CD4+ T cells in the spleen of collagen-induced arthritis (CIA) mice.

Conclusion: By utilizing network pharmacology, molecular modeling, and in vitro/in vivo validation, this study demonstrates that SIN can alleviate RA by inhibiting the PI3K-Akt signaling pathway. These findings enhance the understanding of the therapeutic mechanisms of SIN in RA, offering a stronger theoretical foundation for its future clinical application.

Keywords: sinomenine, rheumatoid arthritis, network pharmacology, PI3K-Akt signaling pathway

Background

Rheumatoid arthritis (RA) is a chronic autoimmune disease primarily affecting the synovial joints. It is characterized by synovitis, pannus formation, and erosion of cartilage and bone, leading to joint deformity, disability, and elevated mortality rates.[1] The prevalence of RA varies globally, but strong trends of increasing RA prevalence over the past three decades.[2] Existing statistical analyses show that RA is not just a medical condition but also a significant public health

Received: 22 May 2024
Accepted: 25 July 2024
Published: 6 August 2024

Graphical Abstract

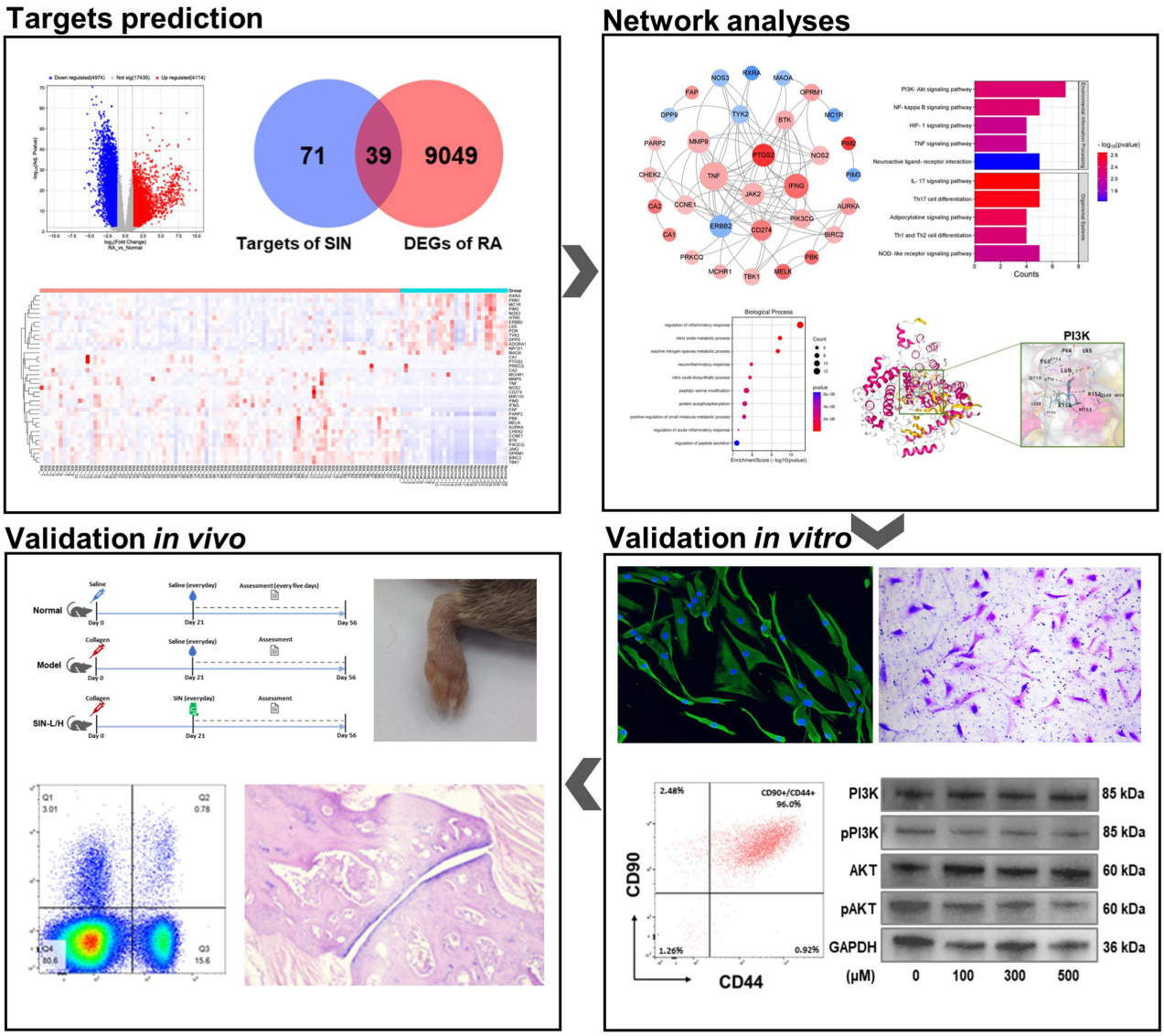

concern.[3] While the mechanisms underlying RA are not completely understood, it is believed that immunological processes occurring in the synovium and synovial fluid play a significant role.[4]

Effective management of RA necessitates prompt initiation of treatment post-diagnosis. Despite this, current disease-modifying anti-rheumatic drugs (DMARDs) are unable to eradicate the disease, and commonly used medications are often associated with notable side effects.[5] Furthermore, certain DMARDs impose significant financial strains on patients without demonstrating proportionate efficacy.[6] Therefore, it is imperative to develop new drugs that are highly effective, cost-efficient, and have minimal side effects.

Traditional Chinese medicine (TCM) has been utilized in the management of RA.[7] Sinomenine (SIN), the primary active compound found in the roots and stems of the plant Sinomenium acutum, is renowned for its effectiveness in treating RA, particularly in East Asia.[8] SIN exhibits multiple pharmacological effects, including anti-inflammatory, analgesic, and immunosuppressive properties.[9] SIN preparations are extensively utilized in clinical practice. A systematic review and meta-analysis consisting of 11 randomized controlled trials (RCTs) illustrated that SIN demonstrates superior

efficacy and fewer side effects compared to methotrexate (MTX) in the treatment of RA[10]. Moreover, another meta-analysis comprising 20 RCTs demonstrated that the combination of SIN with MTX exhibits enhanced effectiveness in treating RA when compared to MTX alone.[11] Although there have been studies on the pharmacological effects of SIN, the molecular mechanisms of its treatment in RA have not been fully elucidated.

Network pharmacology offers a comprehensive understanding of network theory and systems biology. It has been extensively utilized in recent years to predict the active ingredients and mechanisms of action of traditional Chinese medicine.[12,13] Therefore, we conducted network pharmacology and molecular docking analyses to identify the therapeutic targets of SIN against RA. In vitro and in vivo experiments confirmed the proapoptotic and anti-inflammatory effects of SIN in RA, as well as the associated underlying pathways. Our study may contribute to enhancing the understanding of the therapeutic mechanisms of SIN in RA, providing a stronger theoretical foundation for its future clinical application. The technical strategy of the current study is depicted in Figure 1.

Methods and Materials

Chemical Reagents

SIN was obtained from MCE, while Streptomycin/penicillin (P/S) antibiotics and fetal bovine serum (FBS) were procured from Gibco. Trypsin solution and Dulbecco's Modified Eagle Medium (DMEM) were acquired from Hyclone. Primary antibodies (GAPDH, PI3K, p-PI3K, AKT, p-AKT), secondary antibodies conjugated with horseradish peroxidase specific for rabbit IgG, and ELISA kits for mouse IL-1 beta, IL-6, and TNF Alpha were sourced from BOSTER Biological Technology, Co., Ltd in Wuhan, China. Flow cytometry antibodies such as PE anti-mouse/rat/human FOXP3, FITC anti-human CD90 (Thy1), FITC anti-mouse CD4, APC anti-mouse/human CD44, APC anti-mouse CD25, PerCP anti-human CD14, PerCP/Cyanine5.5 anti-mouse IL-17A, APC anti-mouse IFN-γ, and PE anti-mouse IL-4 were purchased from Biolegend. The primary antibody Vimentin was obtained from HuaAn Biotechnology Co., Ltd in Hangzhou, China, and Goat Anti-Rabbit IgG H&L labeled with Alexa Fluor® 488 was acquired from Abcam. Annexin V-FITC/PI apoptosis detection kit and the CCK-8 kit were obtained from Solarbio Science & Technology Co., Ltd, and the cell cycle detection kit was sourced from Bioss Antibodies Co., Ltd, both based in Beijing, China. Transwell cell culture chambers and Matrigel were purchased from Corning and BD Bioscience. Complete Freund's adjuvant and Type II collagen were sourced from Chondrex, Inc. in Washington, USA. The qPCR primers were custom-designed and manufactured by Shanghai exsyn-bioTechnology Co., Ltd, with other qPCR-related reagents purchased from BioRad.

Identification of Potential Target Genes of SIN Therapy for RA

The chemical structure (Figure 2A) and SMILES (Simplified Molecular Input Line Entry Specification) of SIN were retrieved from the PubChem website (https://pubchem.ncbi.nlm.nih.gov/compound/545930). The prediction of targets for SIN was conducted utilizing the TCMSP server (https://tcmspw.com/tcmsp.php), STITCH database (http://stitch.embl.de/), and SwissTargetPrediction database (http://www.swisstargetprediction.ch/). Dataset GSE89408,[14] consisting of 94 samples from rheumatoid arthritis patients and 28 samples from normal synovial tissue, was retrieved from the GEO database (https://www.ncbi.nlm.nih.gov/geo/query/), The analysis of differentially expressed genes (DEGs) related to RA was conducted using the GEO2R online tool (https://www.ncbi.nlm.nih.gov/geo/geo2r/).[15] The criteria for DEGs were defined as an adjusted p-value (Q value) below 0.01 and an absolute log2 (fold change) greater than 1. Common target genes shared between SIN and DEGs were identified as potential therapeutic targets for SIN treatment in the context of RA.

Construction of Protein–Protein Interaction (PPI) Network and Enrichment Analysis

The protein-protein interaction (PPI) network was constructed using the potential targets identified, with the aid of the online tool STRING (accessible at https://string-db.org/), applying a filter criterion of a combined score below 0.4. Subsequently, the interaction data was downloaded and imported into Cytoscape software (version 3.8.0) for network visualization and analysis. Functional enrichment analysis was carried out using the Database for Annotation, Visualization, and Integrated Discovery (6.8, available at http://david.abcc.ncifcrf.gov/).[16] The identification of

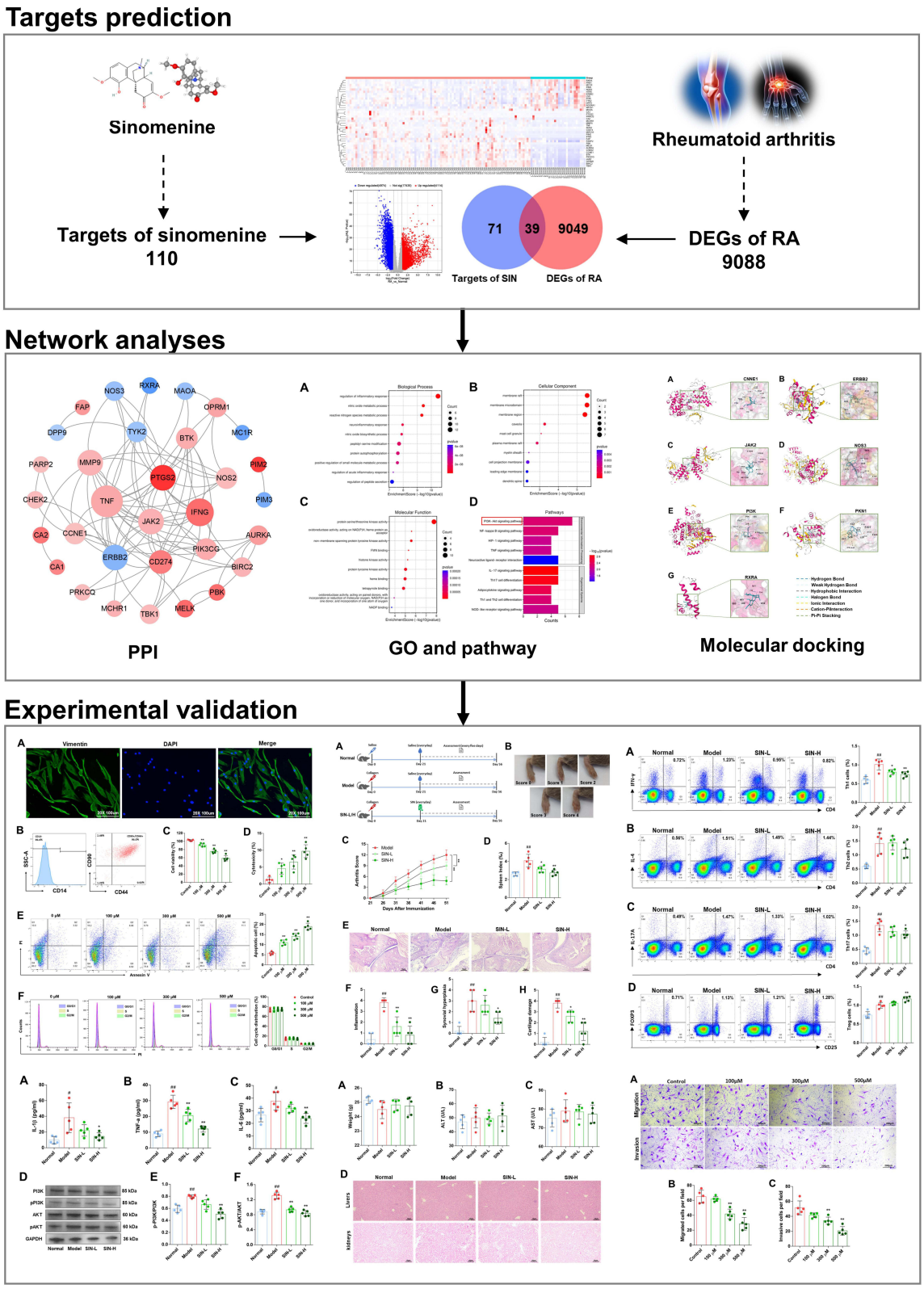

Figure 1 Technical strategy of the current study.

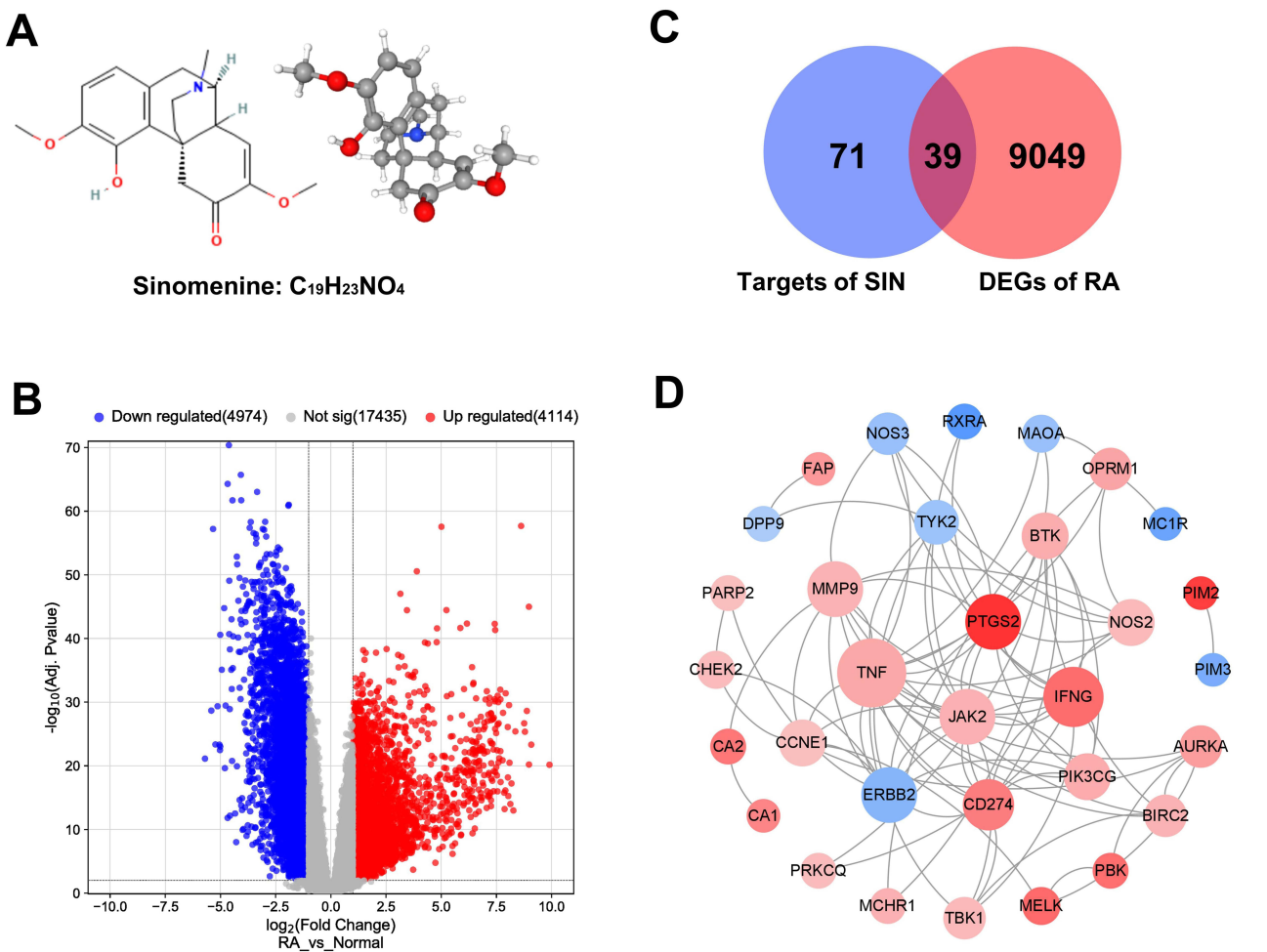

Figure 2 Identification of potential targets for RA therapy with SIN. Chemical structure of SIN (**A**); Venn diagram visualizing the overlap between SIN target genes and DEGs (**B**); Volcano plot illustrating the DEGs between RA and normal samples (Red: Upregulated Genes, Blue: Downregulated Genes) (**C**); Construction of the PPI network for potential targets of SIN in RA (Red: Upregulated Genes, Blue: Downregulated Genes) (**D**); Heatmap depicting the expression of 39 potential targets of SIN in RA (Red: Upregulated Genes, Blue: Downregulated Genes) (**E**).

significantly altered and enriched pathways among the target genes was conducted through the use of the Kyoto Encyclopedia of Genes and Genomes (KEGG).[17]

Molecular Docking

The PDF files of the targets and SDF files of SIN, acquired from the PubChem database (http://pubchem.ncbi.nlm.nih.gov), underwent energy minimization calculations using ChemDraw 3D Ultra software and were saved as mol2 files. Subsequently, these files were uploaded to the CB-Dock website (https://cadd.labshare.cn/cb-dock2/php/index.php).[18] After determining the docking pocket coordinates, we conducted conformational scoring and molecular docking. In the CB-Dock molecular docking framework, lower Vina scores indicated a more stable binding of the ligand to the receptor, enabling the initial evaluation of the binding affinity of the compound with the target.

Isolation and Identification of RA Fibroblast-Like Synoviocytes (RA-FLS)

Five patients with RA who had undergone total knee replacement surgery at Wuxi Ninth People's Hospital Affiliated to Soochow University between February 2023 and July 2023 contributed synovial biopsies for the study. These individuals met the diagnostic criteria outlined by the American College of Rheumatology (ACR) in 2010 and displayed a disease activity score (DAS) exceeding 3.0. This study was approved by the Wuxi Ninth People's Hospital Affiliated to Soochow University Medical Ethical Committee (No. LW20220056), and all patients provided written informed consent. The freshly harvested synovial tissues underwent triple rinsing with phosphate-buffered saline (PBS) and were then cut into 1 mm^3 pieces. Subsequently, the tissues underwent digestion using a 2% type II collagenase solution at a concentration of 1 mg/mL in 3 mL of DMEM. After 4 to 6 hours of digestion, a cell suspension was obtained, which was passed through a 70 μm cell strainer and centrifuged at 1000 rpm for 5 minutes. The resultant pellet was resuspended in DMEM supplemented with 10% FBS. The cells were cultured in a flask and maintained in a 5% CO_2 environment at 37 °C. Flow cytometry and immunofluorescent staining were utilized to identify FLS markers (CD14, CD90, CD44, and Vimentin) for characterization.[19]

Cell Viability Assay

Cell viability was determined using a CCK-8 assay. RA-FLS cells were seeded in a 96-well plate at a density of 3 × 10^3 cells per well and incubated at 37°C for 12 hours. Subsequently, SIN at concentrations of 0, 100, 300, and 500 μM was added, followed by further incubation for 24 hours. Afterward, 10 μL of CCK-8 solution was added, and the cells were incubated for an additional 2 hours. Absorbance at 450 nm (OD450) was then measured.

Assessment of Cytotoxicity

After applying various treatments, the cell culture medium was collected, and the levels of lactate dehydrogenase (LDH) were measured using LDH assay kits (obtained from Beyotime Institute of Biotechnology, Shanghai, China) in accordance with the manufacturer's instructions. Cytotoxicity was assessed with the formula: Cytotoxicity (%) = (Absorbance of treated sample - Absorbance of sample control well) / (Absorbance of maximum enzyme activity in cells - Absorbance of sample control well) × 100.

Apoptosis Analysis

After the cell viability assay, RA-FLS cells were exposed to different concentrations of SIN (0 μM, 300 μM, and 500 μM) in 6-well plates. The control group was treated with an equal volume of saline. Following a 72-hour incubation, cells were harvested, centrifuged, and the cell pellet was resuspended in 400 μL of chilled binding buffer. Subsequently, the cells were stained with 5 μL of Annexin V and 10 μL of PI for 15 minutes in a dark room at room temperature (RT). Cell apoptosis was then analyzed using flow cytometry (Beckman Coulter).

Cell Cycle Analysis

RA-FLS cells were initially seeded in 6-well plates and allowed to grow for 24 hours. Once the cell confluence reached approximately 75%, they underwent 24 hours of serum starvation before being exposed to SIN at concentrations of 0 μM,

300 μM, and 500 μM. After a 48-hour treatment period, the cells were harvested, fixed in ice-cold 75% ethanol overnight at 4 °C, and subsequently washed with PBS. They were then treated with RNase A (100 μg/mL) for 30 minutes at 37 °C. Following the rinse, the cells were stained with 500 μL of PI (50 mg/mL) in the dark for 30 minutes at RT. The stained cells were analyzed using flow cytometry.

Migration and Invasion Assay

A total of 2 × 10^4 RA-FLS cells in serum-free DMEM medium containing varying concentrations of SIN (0 μM, 100 μM, 300 μM, 500 μM) were seeded into the upper chamber of 8.0-μm pore filter migration inserts placed in 24-well cell culture plates. The lower chambers were filled with medium containing 10% FBS (600 μL) serving as a chemoattractant. Following a 24-hour incubation period, non-migrated cells were removed from the filter using a cotton swab, and the remaining cells were fixed in 4% paraformaldehyde for 15 minutes. Subsequently, they were stained with 0.1% crystal violet. The total number of migrated cells in three randomly selected fields at 100 × magnification was quantified. All experiments were independently conducted in triplicate.

For the cell invasion assay conducted in Transwell inserts, the inserts were precoated with 20 μL of 10% Matrigel and incubated at 37°C for 45 minutes. Subsequently, 2 × 10^4 RA-FLS cells in serum-free DMEM medium containing SIN (0 μM, 100 μM, 300 μM, and 500 μM) were seeded. In the lower chambers, 600 μL of medium containing 10% FBS was added as a chemoattractant. Following a 24-hour incubation period, the migrated cells were fixed and stained. The invasion values were reported as the average number of cells that had migrated to the underside of the filters per microscopic field. Three microscopic fields per membrane were examined in triplicate experiments.

RNA Isolation and Real-Time PCR Analysis

RNA from RA-FLS treated or untreated with SIN was extracted using the Trizol reagent from Invitrogen Life Technologies, CA, USA, following the manufacturer's instructions. Initially, a suitable amount of Trizol was added to the harvested cells, followed by transfer of lysed cells to a centrifuge tube for subsequent collection of the supernatant post-centrifugation at 12,000g. Subsequently, chloroform extraction was carried out, and the extracted RNA was precipitated with isopropanol at −70°C. The RNA precipitate was then isolated by centrifugation and dissolved in an appropriate volume of DEPC-treated water. Subsequently, cDNAs were synthesized following the manufacturer's instructions with the Prime Script RT Reagent kit from Takara Biotechnology, Dalian, China. Gene expression levels were quantified utilizing the ABI-7500 Thermal Cycler from Applied Biosystems Inc., CA, USA. Relative gene expression was analyzed using the 2^(-ΔΔCt) method, with the Control group (0 μM SIN concentration) utilized for normalization. The primer sequence is shown in Table S1.

Western Blot Analysis

Protein samples were obtained from RA-FLS and ankle tissues of CIA mouse models using BeyoLytic™ Mammalian Active Protein Extraction Reagent (Beyotime Institute of Biotechnology, Shanghai, China) following the manufacturer's protocol. To achieve this, the appropriate amount of protein extraction reagent, along with protease and phosphatase inhibitors, was added to the collected cell or isolated tissue homogenate. Subsequently, the mixture was thoroughly blended, incubated on ice for 20 min, and then centrifuged at 14,000g and 4°C for 10 min to collect the supernatant for determining the protein concentration. Twenty micrograms of protein lysates were separated by 10% SDS-PAGE and subsequently transferred to a polyvinylidene fluoride (PVDF) membrane. Following a 2-hour blocking period with 5% skimmed milk at RT, specific primary antibodies were added and allowed to incubate overnight at 4° C. After washing with TBST, the blots underwent a 2-hour incubation with goat anti-rabbit secondary antibodies at RT. Protein levels were assessed using the enhanced chemiluminescent (ECL) detection system, with GAPDH as the internal standard. The band density was quantified using Image J software.

Induction of Collagen-Induced Arthritis (CIA) in Mice and Experimental Group Design

DBA/1 mice, aged 6 to 8 weeks, were obtained from Vital River Laboratory Animal Technology Co., Ltd. (Beijing, China) and were housed in a specific-pathogen-free animal room under a 12-hour light-dark cycle at a constant

temperature of 20 ± 0.5°C with unrestricted access to food and water. All animal experiments were ethically approved by the Lab Animal Ethical Committee of Wuxi Ninth People's Hospital Affiliated to Soochow University (NO. KS2023043). We followed the GB/T35892 Guidelines for Ethical Review of Animal Welfare and we also follow the rules of 3R laboratory animal welfare principles. The CIA mouse model was induced following a previously published method.[20] The mice were immunized through a single subcutaneous injection at the base of their tails with an emulsion consisting of complete Freund's adjuvant, chick type II collagen, and M. tuberculosis (2 mg/mL). A total of 20 mice were utilized, randomly allocated as follows: 5 mice for the control group, 5 mice for the CIA model group receiving saline, 5 mice for the Low-dose group (SIN-L), and 5 mice for the High-dose group (SIN-H). SIN powder was dissolved in saline to a concentration of 20 mg/mL, and the SIN-L (50 mg/kg) and SIN-H groups (100 mg/kg) received SIN through intraperitoneal injection once daily starting from the 21st day.[21] After 35 days of drug administration, the mice were sacrificed, and serum and tissue samples were collected.

Arthritis Assessment

Arthritis was evaluated by quantifying the arthritis index through a qualitative scoring system as detailed by Rosloniec et al.[22] The qualitative scoring system ranged from 0 to 4, with a score of 1 representing minimal inflammation and a score of 4 indicating significant erythema and swelling across the entire paw. The arthritis index for each mouse was calculated by summing the scores from all four limbs, with a maximum score of 16 per mouse. Arthritis severity and prevalence were evaluated at five-day intervals, starting from the 21st day post-immunization. Additionally, the spleen index was evaluated according to the protocol delineated by Shi et al.[23] Upon sacrificing the mice, the spleens were collected, rinsed with normal saline, delicately dried with filter paper, and subsequently weighed. The spleen index was calculated using the formula below:

$$\%\,\text{Spleen Index} = \text{grams of Spleen Mass}/\text{grams Body Weight} \times 1000.$$

Enzyme-Linked Immunosorbent Assay Analysis

Mouse blood was collected using the abdominal aortic method. Serum was obtained by centrifugation. The concentrations of IL-1β, IL- 6 and TNF-α in the serum were quantified following the specific ELISA kit instructions.

Histopathological Assessment

Finally, we euthanized the mice using an anesthetic method. The right ankle joint tissues were harvested, fixed in 4% paraformaldehyde for 24 hours, and then subjected to decalcification with 10% EDTA over 24 days. Then, the specimens were embedded in paraffin. Afterward, the tissues were cut into 4μm thick sliced and subjected to staining with hematoxylin and eosin (H&E). Light microscopy was employed to observe and assess the changes. The histopathological evaluation of the joints adhered to established research.[24] Synovial hyperplasia, inflammation, cartilage damage, and pannus were assessed in mouse ankles using the following scoring criteria: normal (0), minimal (1), mild (2), moderate (3), and severe (4). Two independent, blinded observers conducted the assessments.

Evaluation of Toxicity in CIA Mouse Models

When evaluating the toxic effect of SIN on the CIA mouse models, we tracked changes in the mice's body weight, employed ALT (Alanine Transaminase) and AST (Aspartate Aminotransferase) ELISA Kit (FineTest, Wuhan, China) to quantify serum ALT and AST levels as markers of liver toxicity, and concurrently conducted HE histological staining on the liver and kidney tissues of each group of mice to study the impact of different SIN doses.

Flow Cytometric Analyses

The spleens of the euthanized mice were promptly harvested and homogenized to isolate splenocytes. For the evaluation of Th1, Th2, and Th17 cells, 10^7 freshly isolated splenocytes were cultured in 24-well plates at 37 °C with 5% CO2. Stimulation was induced by treatment with ionomycin (1 mM) (Sigma, St. Louis, USA) and PMA (50 ng/mL) for 6 hours. GolgiStop reagent (2 μM) was used to inhibit cytokine secretion, followed by surface staining with FITC-anti-CD4. After fixation and permeabilization, staining with APC anti-IFN-γ, PE anti-IL-4, and PerCP/Cyanine5.5 anti-IL-17A was carried out. For the

detection of regulatory T cells (Tregs) via surface staining, cells were incubated with PE-anti-CD25 and FITC-anti-CD4. Subsequently, intracellular staining was performed by fixing and permeabilizing the cells with PE-anti-Foxp3 antibodies, followed by analysis using a flow cytometer. Data analysis was conducted using FlowJo software from TreeStar.

Statistical Analysis

GraphPad Prism 9 software (GraphPad Software, CA, USA) was used for statistical analysis and graphical representation. Data distribution was evaluated through Q-Q plots, and results were presented as Mean ± SD. Differences among groups were assessed using Welch's ANOVA with the Games-Howell post hoc test. Statistical significance was considered at $P < 0.05$. Sample size was determined following the "resource equation method" guidelines, which indicate 10 to 20 acceptable error degrees of freedom for the ANOVA test. Our experiment samples were divided into four groups, each with five samples, meeting the "resource equation method" requirements.

Results

SIN Treatment of RA Targets Identification

A total of 110 distinct genes were identified as targets of SIN after screening data from the SwissTargetPrediction database, STITCH database, and TCMSP server, following the removal of redundant targets. From the GSE89408 dataset, 9088 DEGs were identified, comprising 4114 upregulated genes and 4974 downregulated genes. The DEG data was visually represented using a volcano plot in Figure 2B. Subsequently, a comparative analysis between the DEGs and potential targets of SIN revealed 39 genes that play crucial roles in the therapeutic efficacy of SIN for treating RA, as depicted in Figure 2C. A network illustrating interactions among proteins encoded by these 39 potential therapeutic target genes was constructed, comprising 85 edges and 32 nodes (Figure 2D). Additional details on these potential targets are presented in Table 1 and visually displayed as a heatmap in Figure 2E.

Table 1 39 Potential Target Genes of SIN Therapy for RA

No.	Target	Symbol	Regulation
1	Prostaglandin-endoperoxide synthase 2	PTGS2	Up
2	Baculoviral IAP repeat containing 2	BIRC2	Up
3	Maternal embryonic leucine zipper kinase	MELK	Up
4	Janus kinase 2	JAK2	Up
5	TANK binding kinase 1	TBK1	Up
6	Pim-2 proto-oncogene, serine/threonine kinase	PIM2	Up
7	Phosphatidylinositol-4,5-bisphosphate 3-kinase catalytic subunit gamma	PIK3CG	Up
8	Aurora kinase A	AURKA	Up
9	Fibroblast activation protein alpha	FAP	Up
10	PDZ binding kinase	PBK	Up
11	Bruton tyrosine kinase	BTK	Up
12	Carbonic anhydrase 2	CA2	Up
13	Checkpoint kinase 2	CHEK2	Up
14	CD274 molecule	CD274	Up
15	Carbonic anhydrase 1	CA1	Up
16	Interferon gamma	IFNG	Up
17	Tumor necrosis factor	TNF	Up
18	microRNA 155	MIR155	Up
19	Protein kinase C theta	PRKCQ	Up
20	poly(ADP-ribose) polymerase 2	PARP2	Up
21	Cyclin E1	CCNE1	Up
22	Opioid receptor mu 1	OPRM1	Up
23	Melanin concentrating hormone receptor 1	MCHR1	Up

(*Continued*)

Table 1 (Continued).

No.	Target	Symbol	Regulation
24	Matrix metallopeptidase 9	MMP9	Up
25	Nitric oxide synthase 2	NOS2	Up
26	Retinoid X receptor alpha	RXRA	Down
27	Lanosterol synthase	LSS	Down
28	Protein kinase N1	PKN1	Down
29	erb-b2 receptor tyrosine kinase 2	ERBB2	Down
30	5-hydroxytryptamine receptor 6	HTR6	Down
31	Melanocortin 1 receptor	MC1R	Down
32	Tyrosine kinase 2	TYK2	Down
33	Pim-3 proto-oncogene, serine/threonine kinase	PIM3	Down
34	Cytochrome p450 oxidoreductase	POR	Down
35	Dipeptidyl peptidase 9	DPP9	Down
36	Adenosine A1 receptor	ADORA1	Down
37	Nitric oxide synthase 3	NOS3	Down
38	Nuclear receptor subfamily 1 group D member 1	NR1D1	Down
39	Monoamine oxidase A	MAOA	Down

KEGG Pathway Enrichment Analysis and GO Term

Through analysis using the DAVID database, we conducted GO analysis on the 39 important therapeutic target genes. The outcomes revealed that these genes were primarily associated with various biological processes (BP), including the regulation of inflammatory response and the nitric oxide metabolic process, among others. In terms of cellular components (CC), significant categories included membrane raft, microdomain, and region. Regarding molecular functions (MF), key categories comprised protein serine/threonine kinase activity, oxidoreductase activity, and non-membrane spanning protein tyrosine kinase activity. Based on KEGG pathway annotations, the most enriched pathways were the PI3K-Akt signaling pathway, NF-kappa B signaling pathway, and HIF-1 signaling pathway. A detailed analysis of the top 10 significantly enriched gene biological functions and pathways is presented in Table 2 and illustrated in Figure 3.

Molecular Docking Results

Given that the PI3K-Akt signaling pathway was notably enriched based on KEGG pathway annotations, we conducted molecular docking analysis of SIN with seven targets (CCNE1, ERBB2, JAK2, NOS3, PI3K, PKN1, and RXRA) associated with this pathway. The analysis revealed binding sites between SIN and the seven targets, with the Vina scores consistently below −6.0 kcal/mol for these interactions, as outlined in Table 3. Visual representation of the binding of SIN to the targets was provided in the 3D map illustrated in Figure 4.

The Proliferation of RA-FLS Was Inhibited by SIN

RA-FLS cells were cultured after being separated from the synovial tissue of RA patients. Immunofluorescence staining confirmed positive vimentin expression in the cells, consistent with fibroblast characteristics (Figure 5A). Flow cytometry results showed that 99.6% of the cultured cells had negative expression of CD14, a specific marker for macrophages, and 96.0% exhibited positive expression of CD44 and CD90, specific markers for fibroblasts (Figure 5B).

To evaluate the effect of SIN on RA-FLS cell proliferation, the cells were treated with different concentrations of SIN for specific time periods. Results from the CCK8 assay showed that as the concentration increased, the cell viability of RA-FLS decreased (Figure 5C). Cell cytotoxicity testing revealed that as the concentration of SIN increased, there was a corresponding rise in LDH release from the cells, suggesting a heightened level of membrane damage (Figure 5D). The flow cytometry analysis revealed a significantly elevated proportion of apoptotic cells in the group treated with SIN when compared to the

Table 2 Enrichment Analyses Results of Potential Target Genes of SIN Therapy for RA (Top 10 Terms of Each Category Were Listed)

Ontology	ID	Description	p-value
BP	GO:0050727	Regulation of inflammatory response	3.3E-11
BP	GO:0046209	Nitric oxide metabolic process	3.69E-10
BP	GO:2001057	Reactive nitrogen species metabolic process	4.73E-10
BP	GO:0150076	Neuroinflammatory response	1.11E-08
BP	GO:0006809	Nitric oxide biosynthetic process	1.3E-08
BP	GO:0018209	Peptidyl-serine modification	1.99E-08
BP	GO:0046777	Protein autophosphorylation	2.42E-08
BP	GO:0062013	Positive regulation of small molecule metabolic process	2.6E-08
BP	GO:0002673	Regulation of acute inflammatory response	5.16E-08
BP	GO:0002791	Regulation of peptide secretion	6.31E-08
CC	GO:0045121	Membrane raft	2.88E-06
CC	GO:0098857	Membrane microdomain	2.94E-06
CC	GO:0098589	Membrane region	3.79E-06
CC	GO:0005901	Caveola	0.000539
CC	GO:0042629	Mast cell granule	0.000828
CC	GO:0044853	Plasma membrane raft	0.001367
CC	GO:0043209	Myelin sheath	0.00376
CC	GO:0031253	Cell projection membrane	0.004332
CC	GO:0031256	Leading edge membrane	0.00472
CC	GO:0043197	Dendritic spine	0.00472
MF	GO:0004674	Protein serine/threonine kinase activity	1.74E-08
MF	GO:0016653	Oxidoreductase activity, acting on NAD(P)H, heme protein as acceptor	2.5E-06
MF	GO:0004715	Non-membrane spanning protein tyrosine kinase activity	2.66E-06
MF	GO:0010181	FMN binding	4.87E-06
MF	GO:0035173	Histone kinase activity	5.91E-06
MF	GO:0004713	Protein tyrosine kinase activity	9.42E-06
MF	GO:0020037	Heme binding	1.05E-05
MF	GO:0046906	Tetrapyrrole binding	1.47E-05
MF	GO:0016709	Oxidoreductase activity, acting on paired donors, with incorporation or reduction of molecular oxygen, NAD(P)H as one donor, and incorporation of one atom of oxygen	0.000118
MF	GO:0050661	NADP binding	0.000204
Pathway	hsa04151	PI3K-Akt signaling pathway	0.005468
Pathway	hsa04064	NF-kappa B signaling pathway	0.005491
Pathway	hsa04066	HIF-1 signaling pathway	0.00889
Pathway	hsa04668	TNF signaling pathway	0.008937
Pathway	hsa04080	Neuroactive ligand-receptor interaction	0.056294
Pathway	hsa04657	IL-17 signaling pathway	0.001292
Pathway	hsa04659	Th17 cell differentiation	0.001531
Pathway	hsa04920	Adipocytokine signaling pathway	0.003286
Pathway	hsa04658	Th1 and Th2 cell differentiation	0.005688
Pathway	hsa04621	NOD-like receptor signaling pathway	0.008457

control group (Figure 5E). Our investigation also included an analysis of the cell cycle of RA-FLS post-SIN treatment. However, the findings indicated that alterations in SIN concentration had no impact on the cell cycle of RA-FLS (Figure 5F).

SIN Suppressed the Migration and Invasion of RA-FLS

RA-FLS were treated with different concentrations of SIN to investigate its impact on cell metastasis and invasion. As illustrated in Figure 6, the number of migrated and invasive cells significantly decreased following SIN treatment compared to the control group (0 μM).

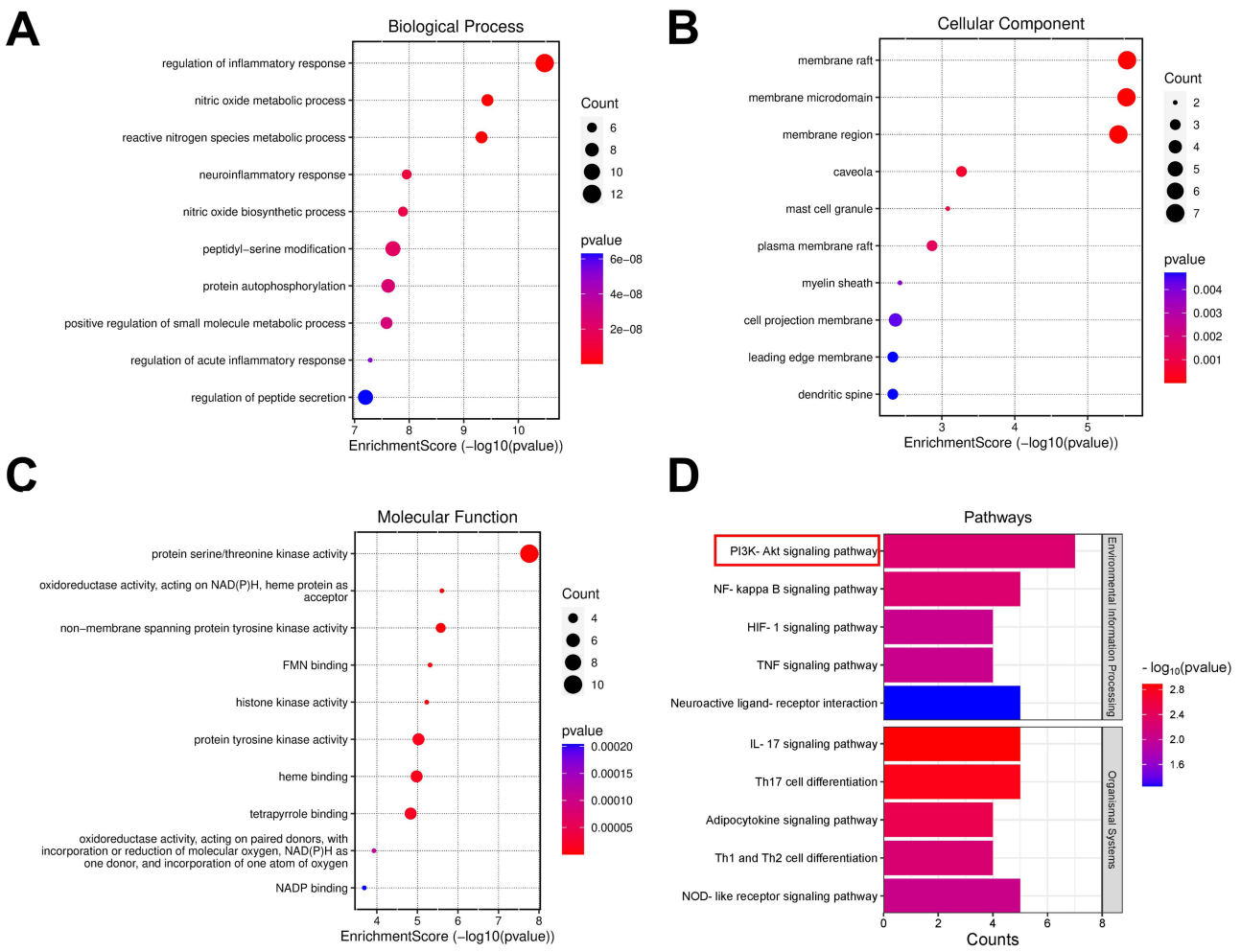

Figure 3 Enrichment Analysis of 39 potential targets of SIN in RA. Gene Ontology (GO) analysis for the identified potential targets, presenting the top 10 GO terms in biological processes (**A**), cellular components (**B**), and molecular functions (**C**), followed by KEGG pathway annotations (**D**).

SIN Suppressed the Production of Inflammatory Cytokines in RA-FLS

In vitro inflammation cell models, IL-1β, IL-6 and TNF-α were chosen as markers to evaluate the extent of inflammation. RA-FLS were exposed to different concentrations of SIN, and the expression of inflammatory cytokines was analyzed using qPCR, normalized to GAPDH. Our results demonstrated the effective suppression of IL-1β, IL-6 and TNF-α expression in RA-FLS by SIN (Figure 7A–C).

Table 3 Molecular Docking Parameters and Outcomes for the Binding of SIN with the 7 Targets Involved in PI3K-Akt Signaling Pathway

Target Name	Vina Scores (kcal/mol)	Cavity Size	Center[a]			Size[b]		
			x	y	z	x	y	z
CCNE1	−6.8	3735	24	−1	18	35	19	31
ERBB2	−7.7	1669	36	40	−13	27	19	30
JAK2	−7.0	4067	93	84	7	25	28	27
NOS3	−7.7	536	23	−2	63	19	19	19
PI3K	−7.6	3415	31	48	37	35	19	32
PKN1	−7.3	603	−15	10	−16	19	19	19
RXRA	−6.3	168	5	−21	29	19	19	19

Notes: [a]Docking pocket center coordinates; [b]The size in the x, y, and z directions of the docking pocket.

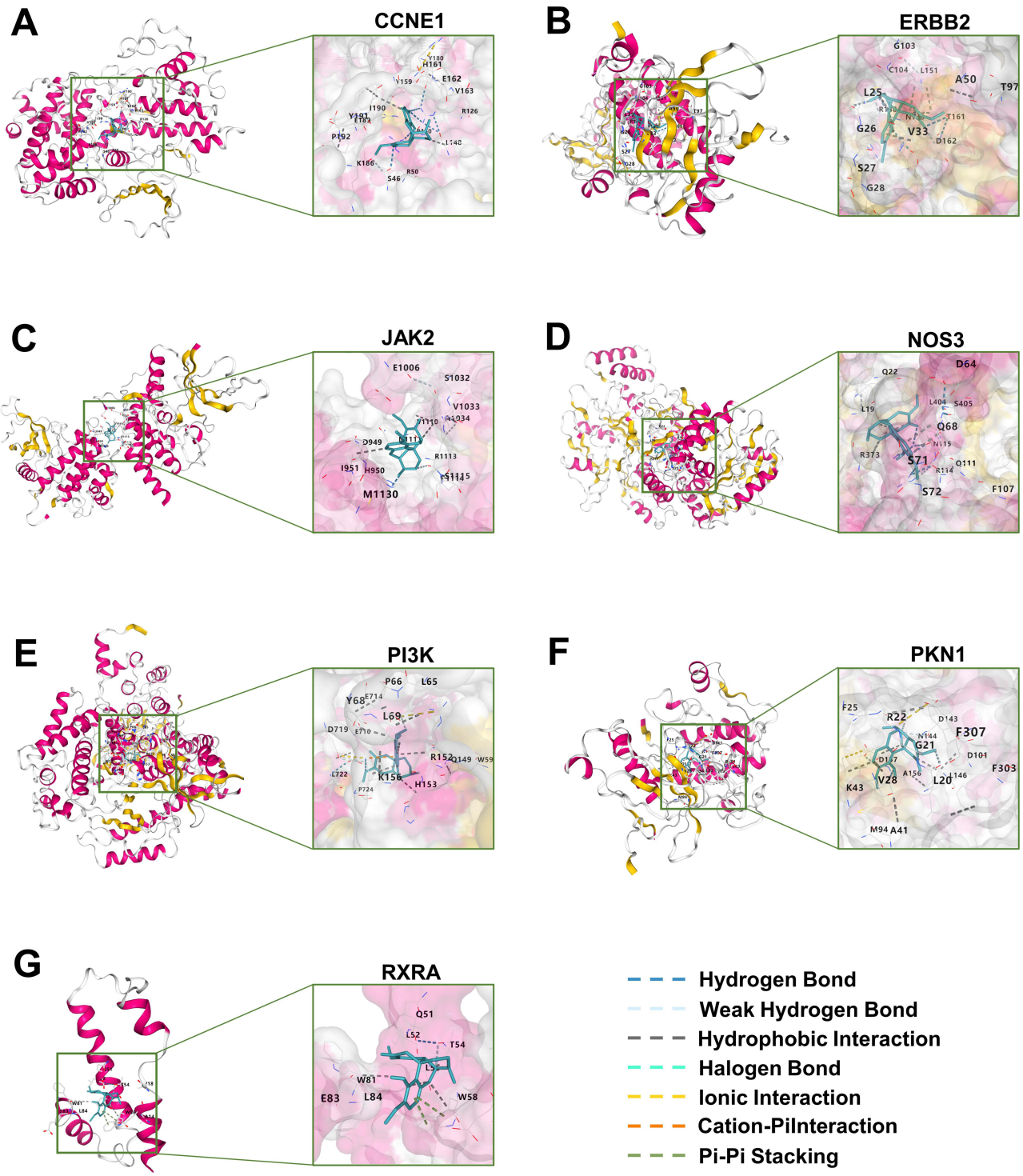

Figure 4 Molecular docking results. The outcomes of the molecular docking analysis revealed that SIN exhibited specific binding with the seven targets, CCNE1 (**A**), ERBB2 (**B**), JAK2 (**C**), NOS3 (**D**), PI3K (**E**), PKN1 (**F**), and RXRA (**G**), that associated with the PI3K-Akt signaling pathway.

SIN Inhibited PI3K-Akt Signaling Cascade in RA-FLS

Given that the enrichment analysis and molecular docking results indicate the drug primarily targets the PI3K-Akt signaling pathway, we utilized Western blot analysis to evaluate the phosphorylation status of key downstream proteins, PI3K and AKT, within this pathway. Our findings showed a dose-dependent decrease in the phosphorylation levels of PI3K and AKT

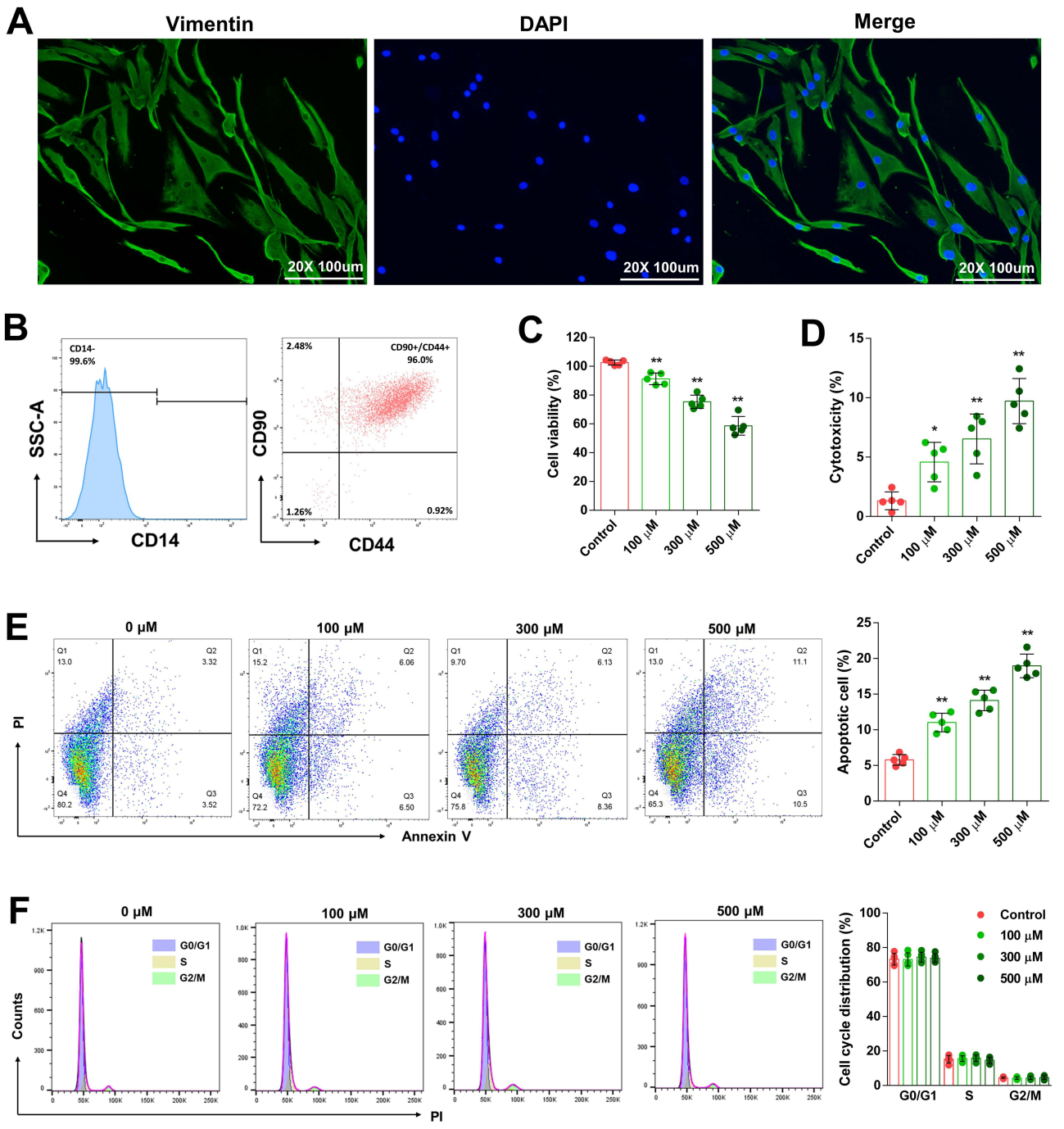

Figure 5 SIN inhibited RA-FLS cells proliferation. Specific markers of RA-FLS were identified through immunofluorescence staining (**A**) and flow cytometry analysis (**B**), Cell viability (**C**) and cytotoxicity (**D**) of RA-FLS after SIN treatments, RA-FLS apoptosis (**E**) and cell cycle (**F**) were analyzed using flow cytometry. The data is presented as the mean ± SEM (n=5), where * and **Indicate significance at *P*-values lower than 0.05 and 0.01, respectively.

in RA-FLS with increasing doses of SIN (Figure 7D–F). We also assessed the mRNA expression levels of seven target genes validated via molecular docking (Figure 7G–M). Our findings revealed that the expression levels of certain downstream targets (CCNE1, ERBB2, PKN1 and RXRA) involved in regulating cell proliferation decreased following SIN intervention.

SIN Treatment Alleviated RA Related Symptoms in CIA Mice

To investigate the impact of SIN on RA in vivo, CIA mouse models were established. The experimental groupings and intervention methods are depicted in Figure 8A. We used a qualitative scoring system to assess the severity of paw

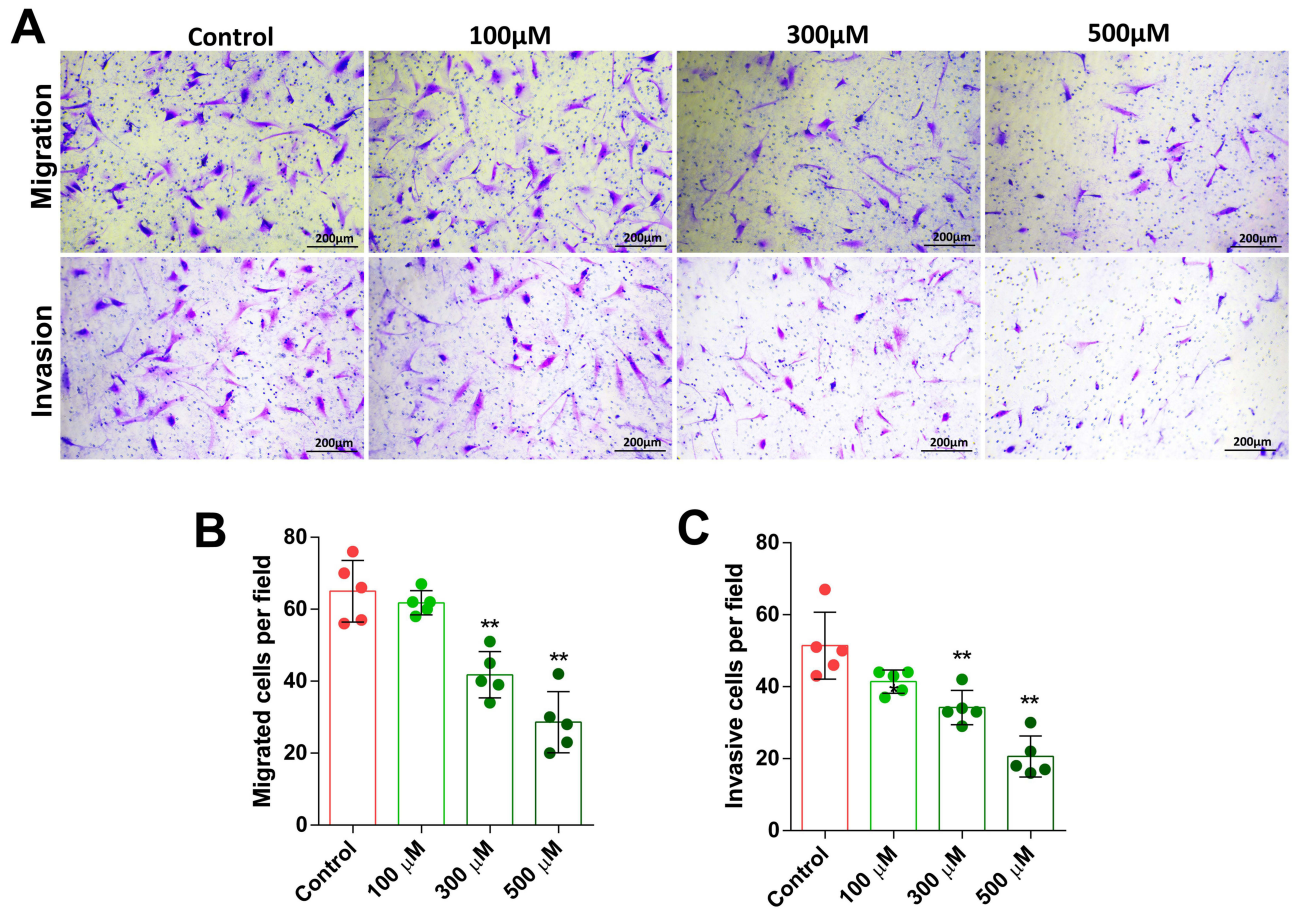

Figure 6 SIN inhibited the migration and invasion of RA-FLS. Representative images of RA-FLS in transwell migration and invasion assays were captured (**A**), Cell migration (**B**) and invasive (**C**) capacity were assessed by cell counting. The data is presented as the mean ± SEM (n=5), where **Indicate significance at *P*-values lower than 0.01.

inflammation, with distinct morphological changes observed at each grade (Figure 8B). The arthritis index score was higher in the CIA model group compared to the control group but lower in the SIN-treated group than in the CIA model group. Moreover, the arthritis index scores of the high-dose SIN treatment group (SIN-H, 100 mg/kg) were lower than those of the low-dose group (SIN-L, 50 mg/kg) (Figure 8C). The spleen index was significantly higher in the model group than in the control group. In contrast, the SIN-treated groups exhibited a substantial decrease in spleen index compared to the model group (Figure 8D). Histopathological analysis of model group revealed significant arthritis-related histopathological changes, such as synovial hyperplasia, inflammatory cell infiltration, and cartilage degeneration, in comparison to the control group. However, SIN treatment alleviated these histopathological alterations in the ankle joints of CIA mice, with notable improvement observed in the high-dose group (Figure 8E–H).

Meanwhile, we assessed the toxicity of SIN in mice models of CIA. Following SIN administration, the body weight of the experimental mice did not exhibit a significant decrease compared to the control group (Figure 9A), and there were no significant increases in serum concentrations of ALT (Figure 9B) and AST (Figure 9C). Histological examination by HE staining did not show noticeable inflammation or histopathological alterations in the livers and spleens of the mice in any of the groups (Figure 9D).

SIN Treatment Suppressed the Production of Inflammatory Cytokines and the PI3K-Akt Signaling Pathway in vivo

Consistent with the findings of in vitro experiments, the concentrations of IL-6, IL-1β, and TNF-α in the serum of CIA mice significantly decreased following treatment with SIN (Figure 10A–C). Additionally, the phosphorylation levels of PI3K and AKT in the joint tissue of the mice were lower compared to those in the untreated model group (Figure 10D–F).

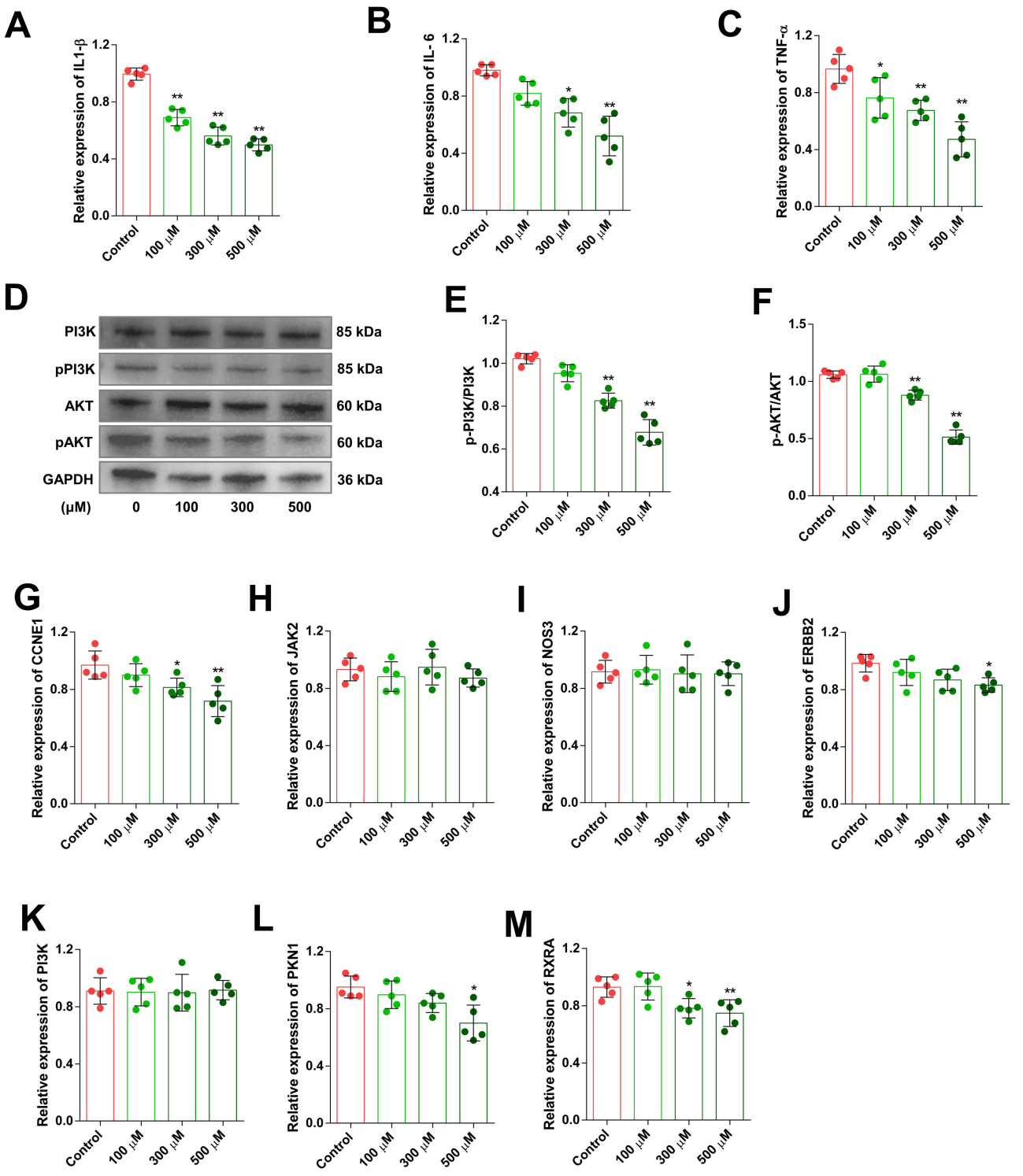

Figure 7 SIN suppressed the production of inflammatory cytokines and the PI3K-Akt signaling pathway in RA-FLS. IL-1β (**A**), IL-6 (**B**), and TNF-α (**C**) expression levels in RA-FLS after SIN treatments were assessed. Western blot detected changes in the phosphorylation of PI3K and AKT in SIN-treated RA-FLS (**D**–**F**). Alterations in the relative expression of CCNE1 (**G**), ERBB2 (**H**), JAK2 (**I**), NOS3 (**J**), PI3K (**K**), PKN1 (**L**), and RXRA (**M**) in RA-FLS following SIN treatment. The data is presented as the mean ± SEM (n=5), where * and **Indicate significance at *P*-values lower than 0.05 and 0.01, respectively.

SIN Modulates the Balance of Th1/Th2 and Th17/Treg Cells in the Spleen of CIA Mice

Flow cytometry was used to assess the impact of SIN on the balance of Th1/Th2 and Th17/Treg cells (Figure 11A). The percentages of Th1, Th2, Th17, and Treg cells in the spleens of mice from all experimental groups were evaluated. SIN

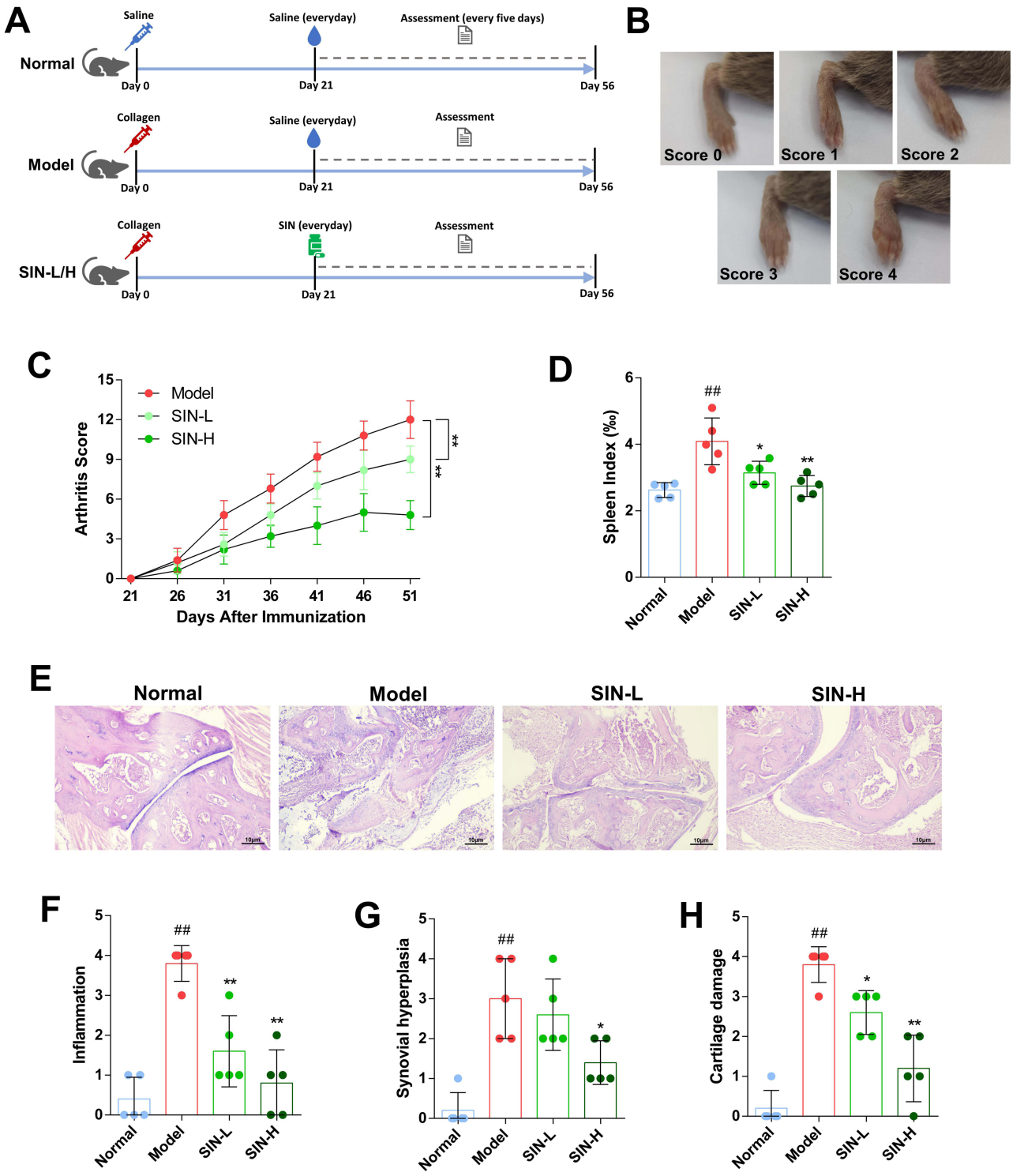

Figure 8 SIN conferred protection to DBA/1 mice against collagen-induced arthritis. Experimental groupings and intervention methods schematic diagram (**A**). Observations of morphological changes in CIA mice for each grade (**B**). Assessment of the arthritis index score in each CIA group (**C**). Measurement of spleen index in mice across all groups (**D**). Illustrative histological staining images of joint tissues (**E**), and inflammation (**F**), synovial hyperplasia (**G**), and cartilage damage (**H**) were evaluated. The data are depicted as mean ± SEM (n=5). The symbols * and **Indicate significance with *P*-values < 0.05 and < 0.01 compared to the CIA group, while ## signifies significance with *P*-values < 0.01 compared to the normal group.

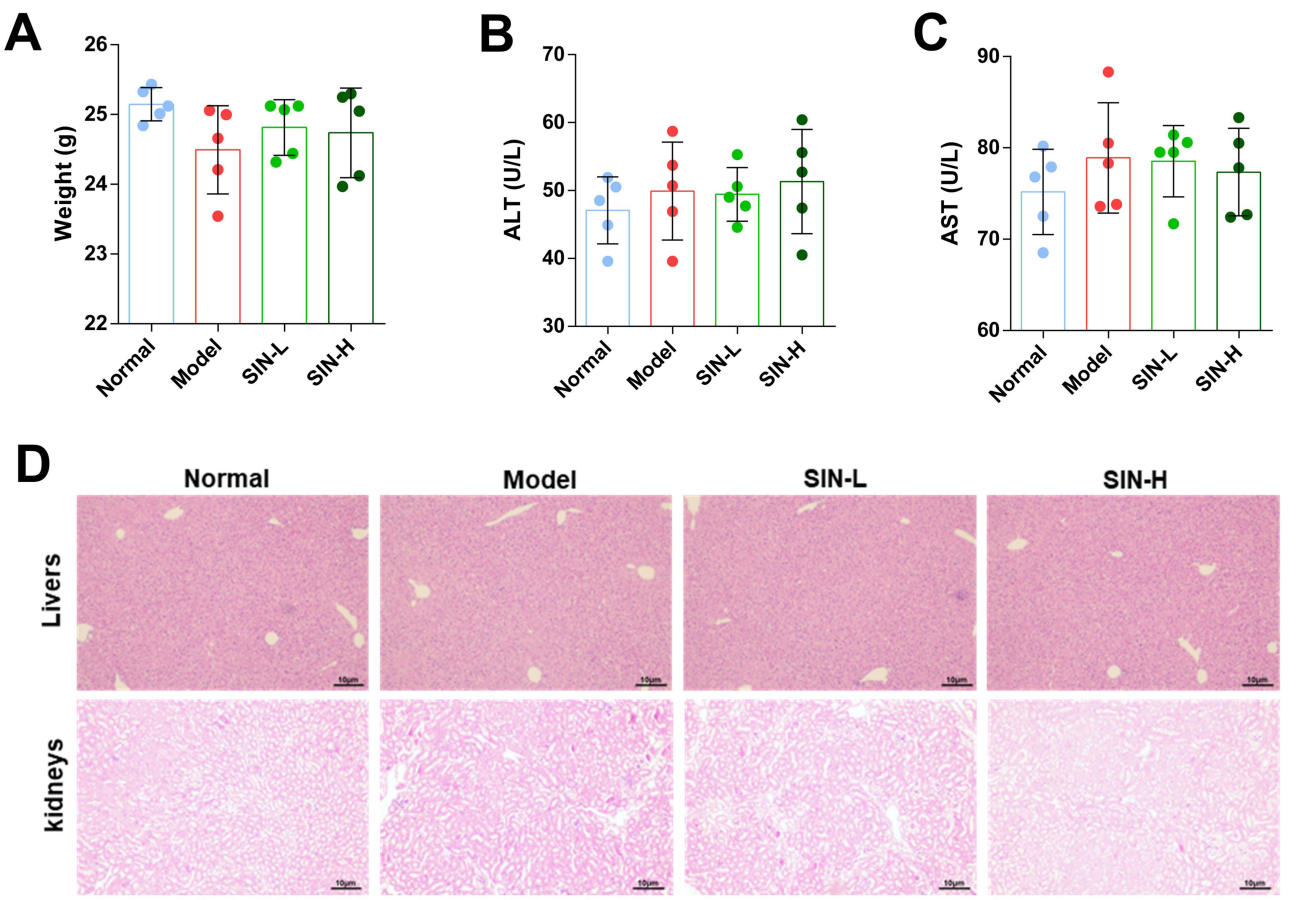

Figure 9 Evaluation of toxicity in CIA mouse models. Following the SIN treatment, alterations in body weight (**A**), serum ALT (**B**) and AST (**C**) concentrations, along with morphological changes in liver and kidney as assessed through immunohistochemical HE staining (**D**).

treatment led to a notable reduction in the proportion of Th1 cells (Figure 11B) without affecting Th2 cells (Figure 11C) significantly. There was no significant alteration in the Th1 to Th2 cell ratio (Figure 11D). Additionally, SIN treatment significantly lowered Th17 cell (Figure 11E) while increasing Treg cell proportions (Figure 11F), consequently reducing the Th17 to Treg cell ratio (G).

Discussion

SIN has been demonstrated to exert a diverse array of pharmacological effects, including anti-inflammatory, immunosuppressive, antitumor, neuroprotective, antiarrhythmic, and other beneficial properties.[25] However, the molecular mechanism of how SIN affects RA remains a topic of debate. This study employed network pharmacology to analyze the associated proteins and signaling pathways involved in the intervention of RA by SIN. Molecular docking and experimental validation corroborated the therapeutic efficacy of SIN against RA.

Initially, we screened 110 potential targets of SIN and identified 9088 DEGs associated with RA from the GSE89408 dataset. Among these, 39 genes were chosen based on the overlap between the targets of SIN and the DEGs, establishing them as potential targets for the therapeutic effects of SIN in treating RA (Figure 2B). The results of the GO enrichment analysis show that the target genes are primarily enriched in the regulation of the inflammatory response, membrane raft composition, and protein serine/threonine kinase activity (Figure 3A–C). These findings will enhance our investigation into the pharmacological effects of SIN. KEGG pathway enrichment analyses revealed that SIN therapeutic targets are primarily enriched in the PI3K-Akt, NF-kappa B, and HIF-1 signaling pathways (Figure 3D). These pathways are intricately linked to inflammatory diseases and play crucial roles in the progression of RA.[26–28] SIN can alleviate various disease-related inflammatory responses, including RA, by inhibiting the NF-kappa B signaling pathway.[29–31] Abnormal

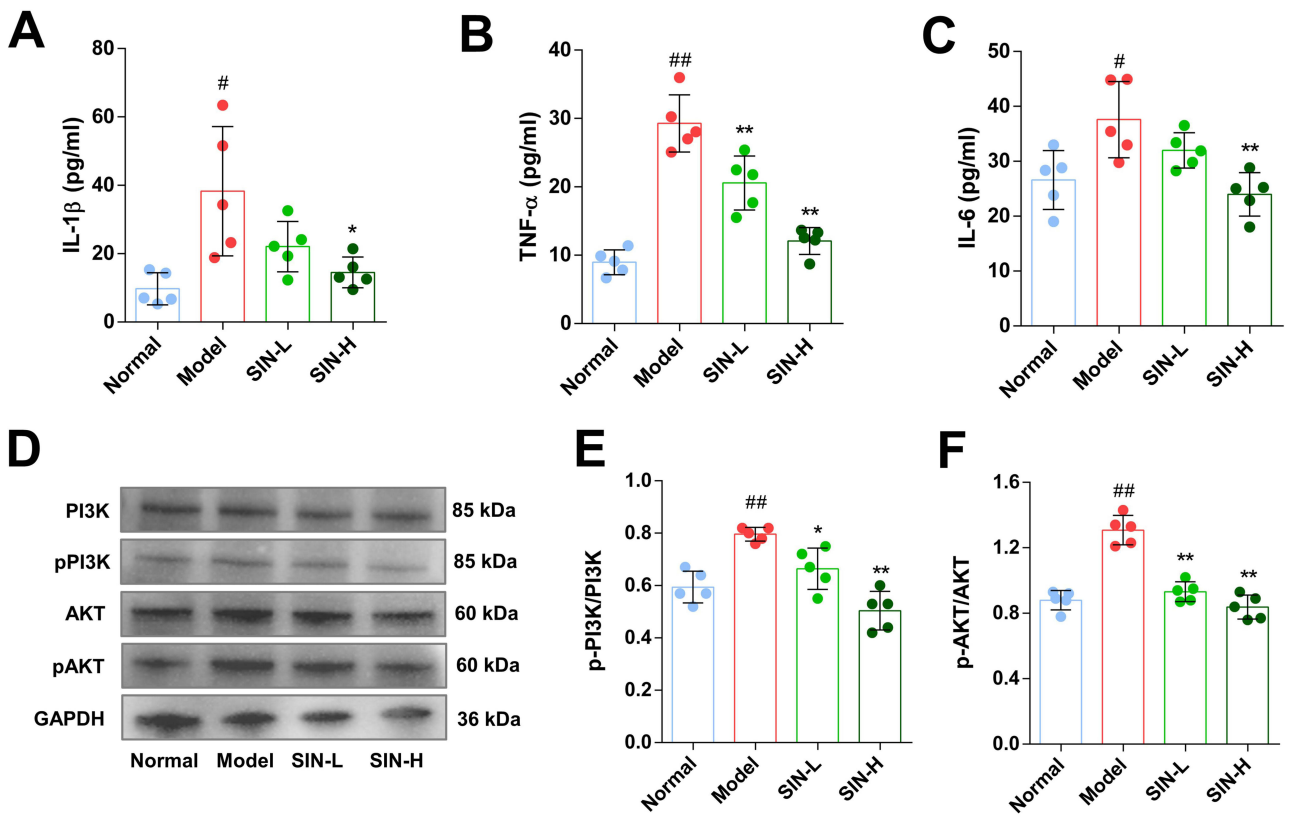

Figure 10 SIN suppressed the release of inflammatory cytokines and inhibited PI3K-Akt signaling pathway in CIA mice. IL-1β (**A**), IL-6 (**B**), and TNF-α (**C**) levels in the serum of mice were determined using ELISA. Western blot detected changes in the phosphorylation of PI3K and AKT in ankle tissues of mouse models (**D–F**). The data are depicted as mean ± SEM (n=5). Symbols *, **, #, and ##Denote significance with P-values < 0.05, < 0.01 compared to the CIA and normal groups, respectively.

expression of hypoxia-inducible factor-1 (HIF-1) in joints is considered a significant factor in initiating the pathological changes seen in RA. Previous research has indicated that SIN can lower the expression levels of HIF-1 in both synovial tissue and serum in animal models.[32,33] The PI3K-Akt signaling pathway has been widely recognized for its involvement in the initiation and advancement of RA.[27] Studies on other diseases have demonstrated that SIN can inhibit the activation of PI3K-Akt signaling pathway.[34–36] However, there is no similar report in RA.

The enrichment analysis results revealed that seven target genes (JAK2, PI3K, CCNE1, ERBB2, NOS3, PKN1, and RXRA) were enriched in the significantly most important signaling pathway, the PI3K-Akt signaling cascade (Figure 3D). Molecular docking was conducted to evaluate the binding of SIN with the seven targets associated with the PI3K-Akt signaling pathway. The outcomes of the molecular docking analysis revealed that SIN exhibited specific binding with each target. Particularly noteworthy is that JAK2, PI3K, ERBB2, NOS3, and PKN1 showed binding affinities below −7.0 (Table 3 and Figure 4). We also investigated the alterations in the expression levels of these target genes in RA-FLS following SIN intervention (Figure 7G–M). The findings revealed a decrease in the expression levels of certain target genes (CCNE1, ERBB2, PKN1 and RXRA) post SIN intervention, primarily situated downstream of the signaling pathway. Based on the aforementioned results, we postulate that SIN could potentially inhibit the activation of the PI3K-Akt signaling pathway by binding to these targets, thus potentially mitigating the advancement of RA.

In order to validate our hypothesis, we utilized RA-FLS to assess the impact of SIN on RA. The CCK8 assay demonstrated a decrease in cell viability of RA-FLS with the increasing concentration of SIN (Figure 5C). Concurrently, the results of the cytotoxicity testing indicated that elevated levels of SIN stimulate cells to release increased amounts of LDH, signifying heightened cellular membrane damage (Figure 5D). We further examined the influence of SIN on apoptosis and the cell cycle of RA-FLS (Figure 5E and F). Some studies have demonstrated the effective inhibition of RA-FLS proliferation by SIN.[37–39] However, confirmation of its association with the PI3K-Akt signaling pathway is still

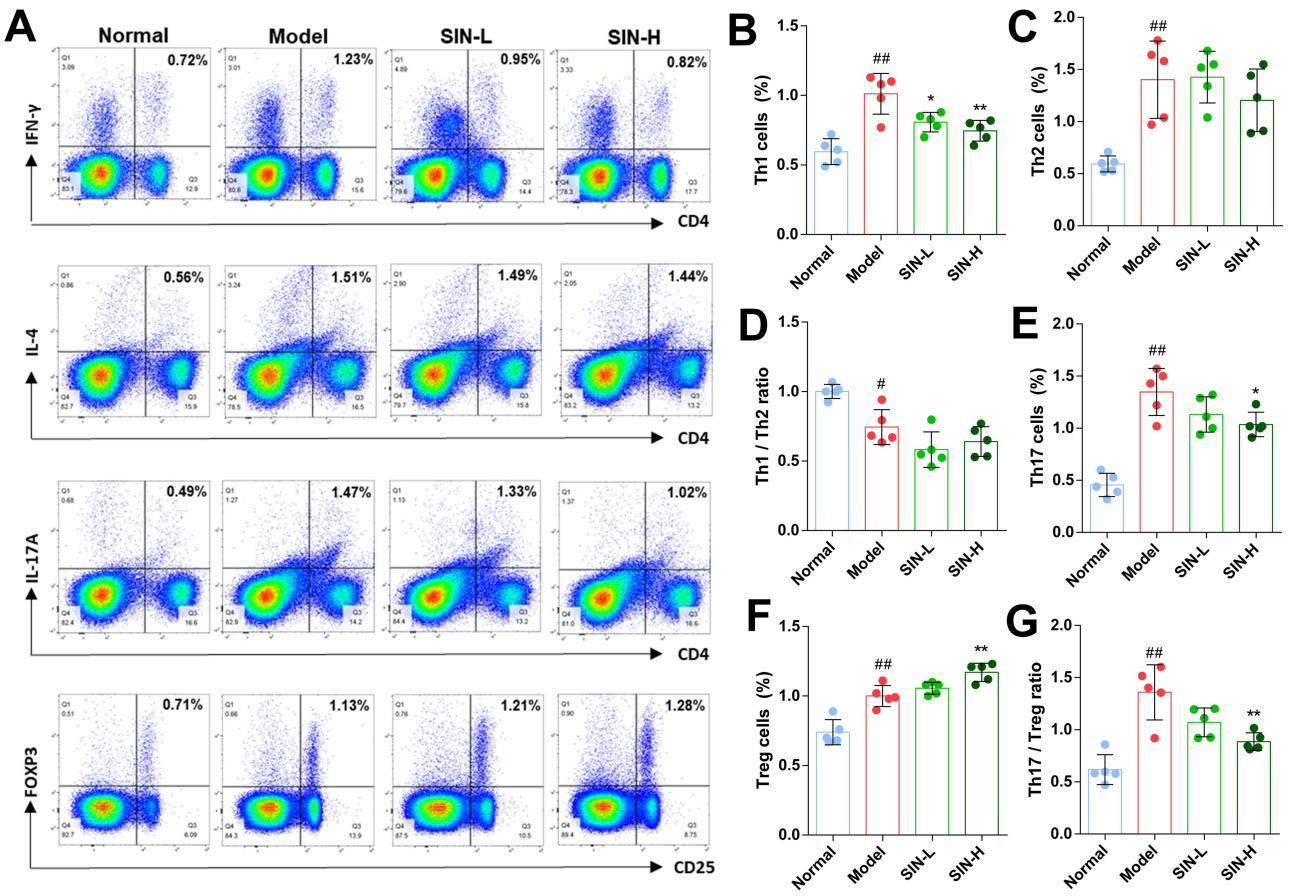

Figure 11 SIN modulates the balance of Th1/Th2 and Th17/Treg cells in the spleen of CIA mice. Representative flow cytometry images of CD4+ T cells were captured (**A**), and the proportions of Th1 cells (**B**), Th2 cells (**C**), the ratio of Th1 and Th2 cells (**D**), Th17 cells (**E**), Treg cells (**F**), and the ratio of Th17 and Treg cells (**G**) were calculated. The data are depicted as mean ± SEM (n=5). Symbols *, **, #, and ##Denote significance with P-values < 0.05, < 0.01 compared to the CIA and normal groups, respectively.

pending. Due to the migration and invasion of FLSs implicated in the development and progression of RA, and considering the confirmed inhibitory effect of SIN on the migration and invasion abilities of various tumor cells,[40–42] we proceeded to investigate the impact of SIN on the migration and invasion of RA-FLS. Figure 6 illustrates that SIN decreased the migratory and invasive capabilities of RA-FLS. These findings indicate that SIN potentially contributes to the treatment of RA by inducing apoptosis and restricting the metastasis and invasion of RA-FLS cells.

Pro-inflammatory cytokines responsible for modulating joint inflammation and damage in RA.[43] Our findings show that SIN proficiently inhibits the production of IL-6, IL-1β, and TNF-α in RA-FLS (Figure 7A–C). Corresponding to the in vitro experimental outcomes, SIN significantly decreased the levels of these cytokines in the serum of CIA mouse models (Figure 10A–C). These findings align with prior studies, which indicating that SIN can hinder the release of pro-inflammatory cytokines in RA patients through diverse mechanisms encompassing methylation, phosphorylation regulation, and the suppression of specific signaling pathways.[25,37,44] Due to the prominence of the PI3K-Akt signaling pathway and its high gene count in enrichment analyses (Figure 3D), we utilized Western blotting to evaluate the phosphorylation levels of PI3K and AKT, key proteins in this pathway, in RA-FLS post-treatment with SIN. The results demonstrate that SIN inhibits the phosphorylation of PI3K and AKT in a dose-dependent manner (Figure 7D–F). Additionally, we assessed the activation of the PI3K-Akt signaling pathway in the mouse models, and akin to the findings in the in vitro experiments, SIN impeded the phosphorylation of PI3K and AKT in CIA mice (Figure 10E and F). These results suggest that the PI3K-Akt signaling pathway could be a target for SIN intervention in the treatment of RA.

The CIA mouse model displays both immunological and pathological resemblances to human rheumatoid arthritis, making it an appropriate model for studying the fundamental mechanisms of RA and evaluating prospective treatments.[22]

In the present study, treatment with SIN led to a decrease in qualitative clinical scores, a reduction in the spleen index of CIA mice, and improvements in joint histopathological changes (Figure 8). These results indicate that SIN offers benefits in alleviating symptoms of RA. Our experimental findings are in line with previous studies demonstrating the effectiveness of SIN and its derivatives in alleviating symptoms in animal models of RA.[21,45] Although SIN is presently utilized in clinical practice for treating rheumatoid arthritis, we conducted an assessment of the impact of SIN treatment on serum enzymes in mouse models, along with examining the morphological alterations in the liver and kidneys. The findings revealed that SIN administration did not result in elevated levels of serum transaminases in mice, nor did it induce any observable pathological changes in liver and kidney cells when examined microscopically (Figure 9).

The dysregulation of CD4+ T cell differentiation is implicated in the pathogenesis of RA, and research indicates that correcting this dysregulation can effectively alleviate symptoms associated with RA.[46,47] Organismal systems enrichment analyses revealed that the therapeutic targets of SIN significantly influence CD4+ T cell differentiation, particularly in Th1, Th2, and Th17 cells (Figure 3D). Therefore, we quantified the counts of Th1, Th2, Th17, and Treg cells in the spleen of the CIA mice. The results indicate that SIN decreased the percentage of Th1 and Th17 cells in the experimental models while increasing the proportion of Treg cells (Figure 11). SIN has been validated to inhibit Th1 and Th2 immune responses in CIA mouse models, and it could also regulate the Th1/Th2 cytokine balance in patients with mesangial proliferative nephritis.[48,49] However, to the best of our knowledge, there is currently no direct evidence that SIN can inhibit the differentiation of CD4+ T cells into Th1 or Th2 cells. Furthermore, animal studies have shown that SIN enhances the differentiation of Treg cells in the gastrointestinal lymphoid tissues and suppresses the proliferation of Th17 cells.[50] Nevertheless, there was no notable variation in the counts of CD4+ CD25+ Foxp3+ T cells in the systemic circulation of RA patients undergoing SIN therapy.[51] Given the discordance between the pharmacological impacts of SIN on CD4+ T cell differentiation in experimental models versus clinical settings, more investigation is warranted to elucidate the regulatory effects of triptolide on CD4+ T cells in RA therapy.

Conclusion

In summary, through the application of network pharmacology, molecular docking, and experimental validation, this study offers an all-encompassing and visual understanding of the potential molecular mechanisms of SIN in RA. Our research revealed that SIN inhibits the activation of the PI3K-Akt signaling pathway, leading to the amelioration of RA symptoms in CIA mice. These findings contribute to the enhanced comprehension of SIN's therapeutic actions in RA, laying a solid theoretical foundation for its prospective clinical utilization.

Ethics Statement

This study was performed in line with the principles of the Declaration of Helsinki and the relevant guidelines and regulations, and was carried out with the consent of patients. Approval was granted by Wuxi Ninth People's Hospital Affiliated to Soochow University Medical Ethical Committee (NO. LW20220056). The animal study was reviewed and approved by The Lab Animal Ethical Committee of Wuxi Ninth People's Hospital Affiliated to Soochow University (NO. KS2023043).

Acknowledgments

This research was supported by Scientific Research Program of Jiangsu Health Commission (H2023093), Top Talent Support Program for young and middle-aged people of Wuxi Health Committee (BJ2023109), Scientific Research Project of Wuxi Municipal Health Commission (Q202237), and the Innovation Project (Ph. D) of Wuxi 9th People's Hospital Affiliated to Soochow University (YB202101-10).

Disclosure

The authors report no conflicts of interest in this work.

References

1. Cush JJ. Rheumatoid arthritis: early diagnosis and treatment. *Rheum Dis Clin North Am*. 2022;48(2):537–547. doi:10.1016/j.rdc.2022.02.010
2. Finckh A, Gilbert B, Hodkinson B, et al. Global epidemiology of rheumatoid arthritis. *Nat Rev Rheumatol*. 2022;18(10):591–602. doi:10.1038/s41584-022-00827-y
3. Littlejohn EA, Monrad SU. Early Diagnosis and Treatment of Rheumatoid Arthritis. *Prim Care*. 2018;45(2):237–255. doi:10.1016/j.pop.2018.02.010
4. Zhao J, Jiang P, Guo S, Schrodi SJ, He D. Apoptosis, autophagy, NETosis, necroptosis, and pyroptosis mediated programmed cell death as targets for innovative therapy in rheumatoid arthritis. *Front Immunol*. 2021;12:809806. doi:10.3389/fimmu.2021.809806
5. Aletaha D, Smolen JS. Diagnosis and management of rheumatoid arthritis: a review. *JAMA*. 2018;320(13):1360–1372. doi:10.1001/jama.2018.13103
6. Huang J, Fu X, Chen X, Li Z, Huang Y, Liang C. Promising therapeutic targets for treatment of rheumatoid arthritis. *Front Immunol*. 2021;12:686155. doi:10.3389/fimmu.2021.686155
7. Liu X, Wang Z, Qian H, et al. Natural medicines of targeted rheumatoid arthritis and its action mechanism. *Front Immunol*. 2022;13:945129. doi:10.3389/fimmu.2022.945129
8. Yamasaki H. Pharmacology of sinomenine, an anti-rheumatic alkaloid from Sinomenium acutum. *Acta Med Okayama*. 1976;30(1):1–20.
9. Li D, Zhong Z, Ko CN, Tian T, Yang C. From mundane to classic: sinomenine as a multi-therapeutic agent. *Br J Pharmacol*. 2023. doi:10.1111/bph.16267
10. Liu W, Qian X, Ji W, Lu Y, Wei G, Wang Y. Effects and safety of Sinomenine in treatment of rheumatoid arthritis contrast to methotrexate: a systematic review and Meta-analysis. *J Tradit Chin Med*. 2016;36(5):564–577. doi:10.1016/s0254-6272(16)30075-9
11. Zeng C, Shuai YF, Li X. [Meta-analysis of efficacy and safety of sinomenine combined with methotrexate in treatment of rheumatoid arthritis]. *Zhongguo Zhong Yao Za Zhi*. 2021;46(1):214–224. doi:10.19540/j.cnki.cjcmm.20200322.501
12. Zhang R, Zhu X, Bai H, Ning K. Network pharmacology databases for traditional Chinese medicine: review and assessment. *Front Pharmacol*. 2019;10:123. doi:10.3389/fphar.2019.00123
13. Zhou Z, Chen B, Chen S, et al. Applications of network pharmacology in traditional Chinese medicine research. *Evid Based Complement Alternat Med*. 2020;2020:1646905. doi:10.1155/2020/1646905
14. Guo Y, Walsh AM, Fearon U, et al. CD40L-dependent pathway is active at various stages of rheumatoid arthritis disease progression. *J Immunol*. 2017;198(11):4490–4501. doi:10.4049/jimmunol.1601988
15. Barrett T, Wilhite SE, Ledoux P, et al. NCBI GEO: archive for functional genomics data sets--update. *Nucleic Acids Res*. 2013;41(Database issue):D991–D995. doi:10.1093/nar/gks1193
16. Dennis G, Sherman BT, Hosack DA, et al. DAVID: database for annotation, visualization, and integrated discovery. *Genome Biol*. 2003;4(5):P3.
17. Kanehisa M, Furumichi M, Tanabe M, Sato Y, Morishima K. KEGG: new perspectives on genomes, pathways, diseases and drugs. *Nucleic Acids Res*. 2017;45(D1):D353–D361. doi:10.1093/nar/gkw1092
18. Liu Y, Grimm M, Dai WT, Hou MC, Xiao ZX, Cao Y. CB-Dock: a web server for cavity detection-guided protein-ligand blind docking. *Acta Pharmacol Sin*. 2020;41(1):138–144. doi:10.1038/s41401-019-0228-6
19. Rosengren S, Boyle DL, Firestein GS. Acquisition, culture, and phenotyping of synovial fibroblasts. *Methods Mol Med*. 2007;135:365–375. doi:10.1007/978-1-59745-401-8_24
20. Brand DD, Latham KA, Rosloniec EF. Collagen-induced arthritis. *Nat Protoc*. 2007;2(5):1269–1275. doi:10.1038/nprot.2007.173
21. Li JM, Deng HS, Yao YD, et al. Sinomenine ameliorates collagen-induced arthritis in mice by targeting GBP5 and regulating the P2X7 receptor to suppress NLRP3-related signaling pathways. *Acta Pharmacol Sin*. 2023;44(12):2504–2524. doi:10.1038/s41401-023-01124-4
22. Rosloniec EF, Whittington K, Proslovsky A, Brand DD. Collagen-induced arthritis mouse model. *Curr Protoc*. 2021;1(12):e313. doi:10.1002/cpz1.313
23. Shi L, Zhao Y, Feng C, et al. Therapeutic effects of shaogan fuzi decoction in rheumatoid arthritis: network pharmacology and experimental validation. *Front Pharmacol*. 2022;13:967164. doi:10.3389/fphar.2022.967164
24. Shen P, Lin W, Ba X, et al. Quercetin-mediated SIRT1 activation attenuates collagen-induced mice arthritis. *J Ethnopharmacol*. 2021;279:114213. doi:10.1016/j.jep.2021.114213
25. Li JM, Yao YD, Luo JF, et al. Pharmacological mechanisms of sinomenine in anti-inflammatory immunity and osteoprotection in rheumatoid arthritis: a systematic review. *Phytomedicine*. 2023;121:155114. doi:10.1016/j.phymed.2023.155114
26. Guo X, Chen G. Hypoxia-inducible factor is critical for pathogenesis and regulation of immune cell functions in rheumatoid arthritis. *Front Immunol*. 2020;11:1668. doi:10.3389/fimmu.2020.01668
27. Prajapati P, Doshi G. An update on the emerging role of Wnt/beta-catenin, SYK, PI3K/AKT, and GM-CSF signaling pathways in rheumatoid arthritis. *Curr Drug Targets*. 2023;24(17):1298–1316. doi:10.2174/0113894501276093231206064243
28. Manou-Stathopoulou S, Lewis MJ. Diversity of NF-kappaB signalling and inflammatory heterogeneity in Rheumatic Autoimmune Disease. *Semin Immunol*. 2021;58:101649. doi:10.1016/j.smim.2022.101649
29. Shen J, Yao R, Jing M, Zhou Z. Sinomenine regulates inflammatory response and oxidative stress via nuclear factor kappa B (NF-kappaB) and NF-E2-related factor 2 (Nrf2) signaling pathways in ankle fractures in children. *Med Sci Monit*. 2018;24:6649–6655. doi:10.12659/MSM.910740
30. Zhou Y, Chen S, Dai Y, et al. Sinomenine attenuated dextran sulfate sodium-induced inflammatory responses by promoting 14-3-3θ protein and inhibiting NF-kappaB signaling. *J Ethnopharmacol*. 2023;303:116037. doi:10.1016/j.jep.2022.116037
31. Yi L, Ke J, Liu J, et al. Sinomenine increases adenosine A(2A) receptor and inhibits NF-kappaB to inhibit arthritis in adjuvant-induced-arthritis rats and fibroblast-like synoviocytes through alpha7nAChR. *J Leukoc Biol*. 2021;110(6):1113–1120. doi:10.1002/JLB.3MA0121-024RRRR
32. Feng ZT, Yang T, Hou XQ, et al. Sinomenine mitigates collagen-induced arthritis mice by inhibiting angiogenesis. *Biomed Pharmacother*. 2019;113:108759. doi:10.1016/j.biopha.2019.108759
33. Li H, Wu QY, Teng XH, et al. The pathogenesis and regulatory role of HIF-1 in rheumatoid arthritis. *Cent Eur J Immunol*. 2023;48(4):338–345. doi:10.5114/ceji.2023.134217
34. Hou W, Huang L, Huang H, et al. Bioactivities and mechanisms of action of sinomenine and its derivatives: a comprehensive review. *Molecules*. 2024;29(2). doi:10.3390/molecules29020540

35. Zhang D, Jin C, Han T, et al. Sinomenine promotes flap survival by upregulating eNOS and eNOS-mediated autophagy via PI3K/AKT pathway. *Int Immunopharmacol*. 2023;116:109752. doi:10.1016/j.intimp.2023.109752
36. Zheng X, Li W, Xu H, et al. Sinomenine ester derivative inhibits glioblastoma by inducing mitochondria-dependent apoptosis and autophagy by PI3K/AKT/mTOR and AMPK/mTOR pathway. *Acta Pharm Sin B*. 2021;11(11):3465–3480. doi:10.1016/j.apsb.2021.05.027
37. Li RZ, Guan XX, Wang XR, et al. Sinomenine hydrochloride bidirectionally inhibits progression of tumor and autoimmune diseases by regulating AMPK pathway. *Phytomedicine*. 2023;114:154751. doi:10.1016/j.phymed.2023.154751
38. Chen DP, Wong CK, Leung PC, et al. Anti-inflammatory activities of Chinese herbal medicine sinomenine and Liang Miao San on tumor necrosis factor-alpha-activated human fibroblast-like synoviocytes in rheumatoid arthritis. *J Ethnopharmacol*. 2011;137(1):457–468. doi:10.1016/j.jep.2011.05.048
39. Sun Y, Ding CZ, Yao Y. [Effects of sinomenine and methotrexate on fibroblast-like synoviocytes in rheumatoid arthritis]. *Zhongguo Zhong Xi Yi Jie He Za Zhi*. 2012;32(8):1107–1111.
40. Song L, Tang L, Lu D, et al. Sinomenine inhibits vasculogenic mimicry and migration of breast cancer side population cells via regulating miR-340-5p/SIAH2 axis. *Biomed Res Int*. 2022;2022:4914005. doi:10.1155/2022/4914005
41. Xu F, Li Q, Wang Z, Cao X. Sinomenine inhibits proliferation, migration, invasion and promotes apoptosis of prostate cancer cells by regulation of miR-23a. *Biomed Pharmacother*. 2019;112:108592. doi:10.1016/j.biopha.2019.01.053
42. Yan J, Yang J, Shen H, Gao R, Lv S. Sinomenine regulates circTRPM7-related pathway to inhibit gastric cancer cell growth and metastasis. *Chem Biol Drug Des*. 2023;102(4):870–881. doi:10.1111/cbdd.14297
43. Edilova MI, Akram A, Abdul-Sater AA. Innate immunity drives pathogenesis of rheumatoid arthritis. *Biomed J*. 2021;44(2):172–182. doi:10.1016/j.bj.2020.06.010
44. Liu W, Zhang Y, Zhu W, et al. Sinomenine inhibits the progression of rheumatoid arthritis by regulating the secretion of inflammatory cytokines and monocyte/macrophage subsets. *Front Immunol*. 2018;9:2228. doi:10.3389/fimmu.2018.02228
45. Lin Y, Yi O, Hu M, et al. Multifunctional nanoparticles of sinomenine hydrochloride for treat-to-target therapy of rheumatoid arthritis via modulation of proinflammatory cytokines. *J Control Release*. 2022;348:42–56. doi:10.1016/j.jconrel.2022.05.016
46. Paradowska-Gorycka A, Wajda A, Romanowska-Prochnicka K, et al. Th17/treg-related transcriptional factor expression and cytokine profile in patients with rheumatoid arthritis. *Front Immunol*. 2020;11:572858. doi:10.3389/fimmu.2020.572858
47. Wang L, Hong X, Du H. Association between serum chemokine ligand 20 levels and disease activity and Th1/Th2/Th17-related cytokine levels in rheumatoid arthritis. *J Interferon Cytokine Res*. 2023;43(11):512–517. doi:10.1089/jir.2023.0057
48. Feng H, Yamaki K, Takano H, Inoue K, Yanagisawa R, Yoshino S. Suppression of Th1 and Th2 immune responses in mice by Sinomenine, an alkaloid extracted from the Chinese medicinal plant Sinomenium acutum. *Planta Med*. 2006;72(15):1383–1388. doi:10.1055/s-2006-951721
49. Cheng Y, Zhang J, Hou W, et al. Immunoregulatory effects of sinomenine on the T-bet/GATA-3 ratio and Th1/Th2 cytokine balance in the treatment of mesangial proliferative nephritis. *Int Immunopharmacol*. 2009;9(7–8):894–899. doi:10.1016/j.intimp.2009.03.014
50. Tong B, Yu J, Wang T, et al. Sinomenine suppresses collagen-induced arthritis by reciprocal modulation of regulatory T cells and Th17 cells in gut-associated lymphoid tissues. *Mol Immunol*. 2015;65(1):94–103. doi:10.1016/j.molimm.2015.01.014
51. Xu W, Chen S, Wang X, et al. Effects of sinomenine on the proliferation, cytokine production, and regulatory T-cell frequency in peripheral blood mononuclear cells of rheumatoid arthritis patients. *Drug Dev Res*. 2021;82(2):251–258. doi:10.1002/ddr.21748